JOURNAL OF GEOPHYSICAL RESEARCH, VOL. 97, NO. C8, PAGES 12,707–12,730, AUGUST 15, 1992

Sensitivities of a Zonally Averaged Global Ocean Circulation Model

DANIEL G. WRIGHT

Department of Fisheries and Oceans, Physical and Chemical Sciences, Bedford Institute of Oceanography Dartmouth, Nova Scotia, Canada

THOMAS F. STOCKER

Lamont-Doherty Geological Observatory, Columbia University, Palisades, New York

A global ocean circulation model is constructed in which the Pacific, Atlantic, Indian, and Southern oceans are separately resolved, each being represented by zonally averaged equations expressing conservation of momentum, mass, heat, and salt. Results are presented and compared with relevant zonally averaged observations. The sensitivity of the stream function and the meridional fluxes of heat and water are examined as functions of the horizontal and vertical diffusion coefficients, and as functions of a closure parameter introduced in averaging the equations. The results are sensitive to changes in the vertical diffusion coefficient and the closure parameter. The sensitivities to changes in the vertical diffusion coefficient are similar to those of a three-dimensional ocean general circulation model. Results are relatively insensitive to the value of the horizontal diffusion coefficient provided it is of the order of 10^3 m^2 s^{-1} or smaller. However, for larger values, a northward heat flux throughout the Atlantic basin, as observed, cannot be obtained. Wind stress significantly improves the comparison with observational estimates of the meridional heat and water fluxes, particularly near the equator, where there are large flux divergences associated with the Ekman transport. Results are further improved when horizontal diffusion is modified to include a contribution proportional to the local current speed. The effects of the Mediterranean and Red seas are examined and shown to be important in redistributing salt vertically. The model is then generalized to allow for depth-integrated flow through the Bering Strait and the Indonesian passages. Both effects improve the comparison with observational estimates, but neither effect appears to be crucial in determining the global circulation or water mass properties in this model. The inclusion of a barotropic flow introduces the necessity to specify a reference temperature in order to calculate the heat flux directly from velocity-temperature correlations. Simply neglecting the barotropic flow may contribute to large discrepancies between flux estimates based on integrated surface fluxes and "direct" correlation methods.

1. INTRODUCTION

Stommel [1961] demonstrated that two stable equilibria occur in a simple system of interconnected reservoirs with density differences sustained by surface heat and salt fluxes. He speculated that similar multiple equilibria may be possible for the global ocean. Probably the most convincing evidence for the existence of such multiple equilibria comes from the interpretations of geochemical observations. For example, *Boyle and Keigwin* [1982, 1987] interpret results from deep-sea sediment cores to suggest that the production of deep water in the North Atlantic was reduced during the last glacial maximum, and *Duplessy et al.* [1988] conclude that Antarctic Bottom Water intruded more strongly into the Atlantic during this period. Further, extensions of Stommel's box model [*Rooth*, 1982; *Welander*, 1986], two-dimensional models [*Marotzke et al.*, 1988; *Wright and Stocker*, 1991; *Stocker and Wright*, 1991*a*, *b*] and numerous studies with ocean general circulation models (OGCMs) [*Bryan*, 1986; *Manabe and Stouffer*, 1988; *Maier-Reimer and Mikolajewicz*, 1989; *Marotzke*, 1989; *Marotzke and Willebrand*, 1991; *Weaver and Sarachik*, 1991*a*, *b*] have exhibited multiple equilibria, and begun to sort out the relevant dynamical processes.

Paper number 92JC01168.
0148-0227/92/92JC-01168$05.00

The primary reason for the great interest in such oceanic (and coupled oceanic-atmospheric) multiple equilibria is the possible significance to climate dynamics. *Broecker and Denton* [1989] present a synthesis of information supporting the idea that the glacial-to-interglacial transitions were accompanied by major reorganizations of the ocean-atmosphere-cryosphere system, and note that the observations cannot be explained without consideration of the oceanic influence. Unfortunately, the coupled system is very complex, and detailed, process-oriented studies are required to build our understanding of it. There is a clear need for models of the climate system which can realistically represent the important components and still be run for periods of many thousands of years. The present paper considers an ocean model which is well suited to this need. Our primary aim is to develop low-order climate models which, through their simplicity, may help clarify the controlling mechanisms of the climate system and provide a context in which many of the complex interactions occurring within this system may be efficiently studied.

Wright and Stocker [1991] (henceforth WS91) developed a zonally averaged model for the thermohaline circulation and demonstrated that it yields results consistent with previous two- and three-dimensional models for isolated ocean basins. The model was extended by *Stocker and Wright* [1991*a*] (henceforth SW91*a*) to allow for two interconnected basins and used to study the global conveyor belt circulation

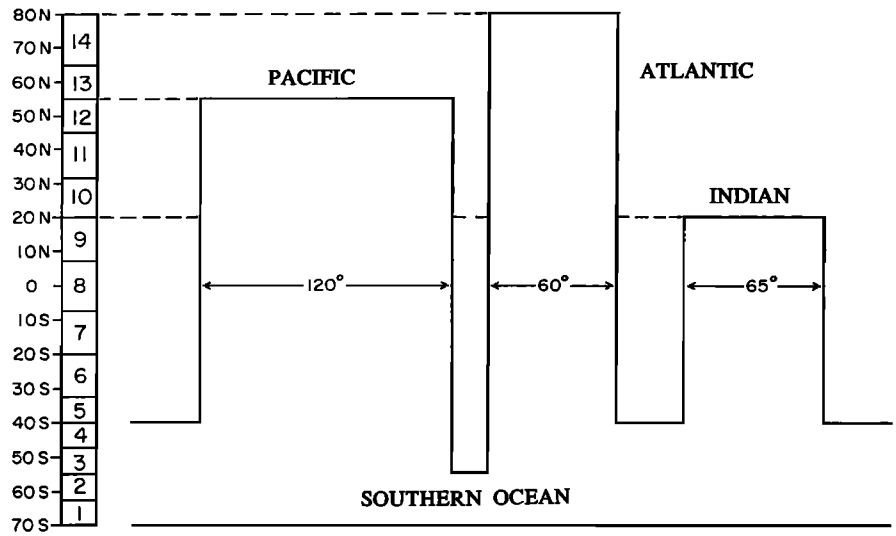

Fig. 1. The idealized model representation of the global ocean. The Pacific, Atlantic, and Indian oceans are represented by 8, 10, and 5 latitude bands as indicated. The Southern Ocean occupies the southernmost four latitude bands, but the extension of South America across part of this region is accounted for through the choice of ε. The basic geometry has a flat bottom, and neither the Arctic Ocean nor the Weddell and Ross seas are included.

which exists today [*Gordon*, 1986], and its stability with respect to freshwater anomalies added to the North Atlantic. Results were encouragingly consistent with observations of global water mass properties [*Levitus*, 1982] and with simulations of more complex OGCMs [*Bryan*, 1986; *Maier-Reimer and Mikolajewicz*, 1989]. Further, the model is computationally efficient; the runs presented here require approximately 5 min CPU per 100 years of simulation on an IBM RISC 6000 work station.

The first purpose of this paper is to present an extended version of our model, which includes a well-mixed surface layer, the influence of wind stress, the Indian Ocean, and a meridional ridge in the Southern Ocean.

The second purpose is to continue our investigation of the physical properties of the model. As already mentioned, it has been shown that it can reproduce the major features of the present-day ocean, and it exhibits multiple equilibria and mode transitions similar to those seen in OGCMs. We now perform a parameter sensitivity study to show that the model also responds to changes in its internal parameters in a manner similar to more complete OGCMs [*Bryan and Lewis*, 1979; *Bryan*, 1987]. This exercise helps establish a foundation for future studies as well as providing a "feel" for the model. In particular, we will examine the sensitivity of the meridional stream function and the meridional heat and water fluxes to variations in the horizontal and vertical diffusion coefficients, and to variations in the closure parameter ε, which arises as a result of zonally averaging the momentum equations. The overturning stream function is a good measure of the influence of our closure scheme, and the sensitivities to the meridional fluxes of heat and salt are of particular interest due to our aim of developing an ocean model suitable for use in long-term, global climate studies.

The final purpose of the paper is to demonstrate the significance of various model simplifications which have been made in our previous (and other) studies. In particular, we will study the influences of wind stress, exchange with the Mediterranean and Red seas, and flow through Bering Strait and the Indonesian passages. The influence of wind stress is clearly important to the determination of the meridional heat and water fluxes carried by the ocean. The other effects improve details of the model solution, but their significance in the global climate system is not yet clear.

The general plan of the paper is as follows. In section 2, the basic model is briefly described, with the modifications to include wind stress, a well-mixed surface layer, and the Indian Ocean influence. An example solution is presented and compared with observations in section 3. In section 4 the sensitivities to variations in the friction and closure parameters are discussed, and results are used to demonstrate how this and previous models may be "tuned" through appropriate choices of uncertain parameters. The influence of wind stress is considered in section 5. Vertical exchange associated with the Mediterranean and Red seas, and the influences of depth-integrated interbasin exchanges are considered in section 6. Results are summarized in section 7.

2. Model Description

To model the global ocean circulation, an idealized ocean model is constructed consisting of three zonally averaged ocean basins, representing the Pacific, Atlantic, and Indian Oceans, connected through a circumpolar basin representing the Southern Ocean (Figure 1). Within each individual basin, the model formulation is as described by WS91, with modifications to include surface and bottom stresses and a well-mixed surface layer (not a mixed layer model). A brief outline of the model formulation emphasizing the new aspects of the model is given below. The reader is referred to WS91 and SW91*a* for further details.

Bottom stress was included through the use of an Ekman drag law [*Gill*, 1982, section 9.6], but due to the smallness of near-bottom currents, its influence was found to be negligible, and hence will not be discussed further. Surface wind stress was included through the specification of the zonally averaged zonal stress τ^s acting on the surface of the ocean: the corresponding meridional stress was not considered. Since the Ekman layer is thinner than the specified surface

layer thickness of 50 m, and since there is no vertical resolution within the surface layer, the inclusion of the surface stress amounts to specifying the Ekman flux to be carried by this uppermost layer. Although results were actually determined through a boundary layer analysis as discussed in WS91, we will simplify the presentation by representing the wind stress through an Ekman flux imparted to the surface layer from the outset. Note that the total velocity in the surface layer is the sum of the Ekman and geostrophic contributions.

The zonally averaged model equations are

$$-2s\Omega\bar{v} = -\frac{1}{\rho_* ac}\frac{\Delta p}{\Delta\Lambda} + \frac{\tau^s}{\rho_* H_M}\mathcal{H}(z + H_M) \tag{1}$$

$$2s\Omega\bar{u} = -\frac{1}{\rho_* a}\frac{\partial\bar{p}}{\partial\phi} \tag{2}$$

$$\frac{\partial\bar{p}}{\partial z} = -\bar{\rho}g \tag{3}$$

$$\frac{1}{ac}\frac{\partial}{\partial\phi}(c\bar{v}) + \frac{\partial}{\partial z}(\bar{w}) = 0 \tag{4}$$

$$\frac{\partial\bar{T}}{\partial t} + \frac{1}{c}\frac{\partial}{\partial\phi}\left(\frac{c\bar{v}}{a}\bar{T}\right) + \frac{\partial}{\partial z}(\bar{w}\bar{T}) = \frac{1}{c}\frac{\partial}{\partial\phi}\left(\frac{cK_H}{a^2}\frac{\partial\bar{T}}{\partial\phi}\right) + \frac{\partial}{\partial z}\left(K_V\frac{\partial\bar{T}}{\partial z}\right) + q_T^{\text{conv}} \tag{5}$$

$$\frac{\partial\bar{S}}{\partial t} + \frac{1}{c}\frac{\partial}{\partial\phi}\left(\frac{c\bar{v}}{a}\bar{S}\right) + \frac{\partial}{\partial z}(\bar{w}\bar{S}) = \frac{1}{c}\frac{\partial}{\partial\phi}\left(\frac{cK_H}{a^2}\frac{\partial\bar{S}}{\partial\phi}\right) + \frac{\partial}{\partial z}\left(K_V\frac{\partial\bar{S}}{\partial z}\right) + q_S^{\text{conv}} \tag{6}$$

$$\bar{\rho} = \bar{\rho}(\bar{T}, \bar{S}, \bar{p}) \tag{7}$$

where ϕ is the latitude, $s = \sin\phi$, $c = \cos\phi$, $\Delta\Lambda$ is the angular width of the basin, and z is the (dimensional) vertical coordinate, increasing from $-H$ at the bottom to zero at the surface; H_M is the mixed layer depth (=50 m here), and $\mathcal{H}$ is the Heaviside unit step function (zero for negative argument and 1 for positive argument); u, v, and w are the horizontal and vertical velocity components; K_H and K_V are the horizontal and vertical diffusion coefficients; q_T^{conv}, q_S^{conv} represent the influence of convective mixing; T, S, ρ, and p denote potential temperature referenced to the surface, salinity, in situ density, and pressure; ρ_* is a constant reference density, Ω and a are the angular velocity and radius of the Earth, and g is the acceleration due to gravity. In the present version we use the fully nonlinear equation of state given by *Gill* [1982]. The overbar represents a zonal average and is dropped henceforth.

Horizontal diffusion of momentum does not appear at all in (1) and (2), and vertical diffusion appears only through the inclusion of the surface Ekman flux. It should be noted that this does not imply that momentum diffusion is unimportant in determining zonally averaged oceanic conditions. Indeed, some form of momentum diffusion is certainly important in determining the structure of eastern and western boundary currents, and these currents do influence zonally averaged conditions. In the present formulation, the dynamics of both eastern and western boundary layers are represented solely through the relation between the east-west density difference and the north-south density gradient discussed below.

The zonally averaged east-west pressure gradient

$$\frac{\Delta p}{\Delta\Lambda} = \frac{p(\lambda_E, s, z) - p(\lambda_W, s, z)}{\lambda_E - \lambda_W} \tag{8}$$

where λ_E and λ_W are the longitudes of the eastern and western boundaries of the basin, cannot be determined from the zonally averaged equations of motion. In the absence of wind forcing, WS91 show that $\Delta p/\Delta\Lambda$ may be approximated by the relation

$$\frac{\Delta p}{\Delta\Lambda} = -\varepsilon\sin(2\phi)\frac{\partial p}{\partial\phi} \tag{9}$$

where ε is a closure parameter. Taking the vertical derivative of (9) gives a more general condition which makes no assumptions about the depth-averaged pressure field:

$$\Delta\rho = -\varepsilon\Delta\Lambda\sin(2\phi)\frac{\partial\rho}{\partial\phi} \tag{10}$$

SW91*a* argue that in a wide basin, the relation between the north-south density gradient and the density difference across the basin should be independent of the basin width, leading to the conclusion that ε should be inversely proportional to the basin width, i.e.,

$$\varepsilon = \varepsilon_0\pi/(3\Delta\Lambda) \tag{11}$$

where ε_0 is the value of ε appropriate to a basin which is 60° wide. Comparisons with an OGCM solution shown in WS91 indicates that ε_0 is of the order of 0.3. Using the hydrostatic relation in the left side of (10), then integrating from the surface to an arbitrary level z, we obtain the relation

$$\frac{\Delta p}{\Delta\Lambda} = \left.\frac{\Delta p}{\Delta\Lambda}\right|_{sfc} - 2\varepsilon scg\int_z^0 \rho_\phi\, dz \tag{12}$$

Equation (12) determines the vertical structure of the geostrophic component of the north-south flow. The model dynamics are then closed under the rigid-lid approximation by the condition that the net north-south transport vanishes at all latitudes. This determines the depth-independent contribution to the north-south velocity, which is in geostrophic balance with the surface pressure gradient.

No-flux conditions are specified for T and S at solid boundaries, and surface layer values are relaxed to observations through the conditions

$$-K_V T_z = \frac{H_M}{\tau_H}(T - T^*) \tag{13}$$

$$-K_V S_z = \frac{H_M}{\tau_S}(S - S^*) \tag{14}$$

where $\tau_H = \tau_S = 50$ days, and T^*, S^* are the zonally averaged values of T and S for the individual basins at 30 m given by *Levitus* [1982].

The incorporation of wind stress in (1) is intended primarily to allow for the direct influence of the surface Ekman

flux on the meridional transport of heat and salt within the surface layer. The vertically integrated fluxes depend on the vertical structure of the return flow and this is determined by (1), (3), and (10). The wind stress influences the vertical structure of this flow through its effect on the density field, and as we shall see, this results in a surface intensification of the wind-driven meridional circulation generally consistent with results of OGCMs.

However, it is important to realize that the depth-integrated, wind-driven horizontal gyre circulation is neglected in the present formulation. In particular, (10) neglects the effect on $\Delta\rho$ of north-south advection by the horizontal gyre circulation [*Ikeda*, 1987], and net north-south heat and salt fluxes associated with correlations between this circulation and east-west temperature and salinity differences are also neglected. The latter effect may be particularly important in the Pacific Ocean, where direct observations across 24°N suggest that the horizontal circulation carries about half of the northward heat transport [*Bryden et al.*, 1991]. This contrasts with results for the Atlantic, where observations at the same latitude indicate that the north-south heat flux is dominated by the meridional overturning circulation [*Hall and Bryden*, 1982].

Within the Southern Ocean the model formulation is exactly the same as described above. Water, heat, and salt are exchanged between the Southern Ocean and the three basins to the north across 40°S. A zonal barrier extends from 40°S to 55°S which can support an east-west pressure gradient parameterized by (9), exactly as in the interior of the basins north of 40°S. Where no barrier to zonal flow is present, ε is chosen to have the very small value of 0.0001. Referring to Figure 1, we see that with the present meridional resolution, there is actually only one latitude at which this small value applies.

In the original model (WS91) a uniform grid was used in both vertical and horizontal directions. Surface values of temperature and salinity (required in the relaxation boundary conditions) were obtained from a linear extrapolation based on the interior values of the upper two layers. This could be a poor approximation, particularly if coarse vertical resolution is considered. To achieve an improved approximation, two changes were made. First, spatially varying horizontal and vertical resolution were allowed for. The chosen horizontal resolution is indicated in Figure 1, and the vertical cell boundaries are located at 50, 100, 150, 250, 500, 750, 1000, 1250, and 1500 m, and at 500-m intervals beneath this depth. Second, the 50-m-thick surface layer has the special property that its temperature and salinity are assumed to be vertically uniform. Except for the fact that this layer is well mixed and carries the Ekman flux, it is dynamically the same as any other layer in the model.

Before considering detailed numerical results, we point out a simple relationship between the velocity and density fields. First, substitution of (12) into (1), integrating the resulting expression for v over the depth of the fluid, and setting the result equal to zero (a consequence of the rigid lid approximation) gives

$$\left.\frac{\Delta p}{\Delta\Lambda}\right|_{sfc} = \frac{1}{H}\left\{2\varepsilon scg\int_{-H}^{0}(z+H)\rho_\phi\,dz + ac\tau\right\} \tag{15}$$

Using (1), (12), and (15), we obtain

$$v = \frac{\varepsilon g}{\Omega H a}\left\{\int_{-H}^{0}\frac{\rho_\phi}{\rho_*}(z+H)\,dz - \int_{z}^{0}\frac{\rho_\phi}{\rho_*}H\,dz\right\} - \frac{\tau^s}{2\Omega\rho_* s}\left(\frac{\mathcal{H}(z+H_M)}{H_M} - \frac{1}{H}\right) \tag{16}$$

Finally, from (4), a stream function exists such that

$$v = -\frac{1}{c}\frac{\partial\psi}{\partial z} \tag{17a}$$

$$w = \frac{1}{ac}\frac{\partial\psi}{\partial\phi} \tag{17b}$$

Integrating (17*a*) gives an analytical expression for ψ from which w is easily obtained using (17*b*).

Note that the first term in (16) indicates a tendency for surface flow towards regions of relatively dense near-surface water as required to supply water to regions of deep convection. The two terms in the braces also give the associated geostrophic return flow. The term proportional to τ^s represents the Ekman flux in the surface layer plus a compensating depth-independent, geostrophic return flow. It should be emphasized that the advective fluxes associated with the wind stress will influence the density field, which changes the vertical structure of the geostrophic interior flow. Thus, one cannot determine the influence of the wind stress from the second term alone.

The solution procedure is essentially as described in WS91. The temperature and salinity fields are updated using forward time-differencing based on (5) and (6). Numerical diffusion associated with the advective terms is reduced using the method developed by *Smolarkiewicz* [1983, p. 480]. Generalizing to a spatially variable grid, his approach gives, for the boundary between cells i and $i+1$,

$$K_H^{\text{num}} = 0.5\left(\frac{|v|+v}{2}\,ad\phi_i + \frac{|v|-v}{2}\,ad\phi_{i+1} - v^2\,dt\right) \tag{18}$$

where $d\phi$ and dt are the angular and temporal increments used in our finite difference approximation. (This formula reduces to his if $d\phi_i = d\phi_{i+1}$ and we convert to a local Cartesian coordinate system.) The expression for the corresponding vertical diffusion coefficient is precisely analogous to (18) with v replaced by w and $ad\phi$ replaced by dz. The density field is determined from (7), and any unstable regions are mixed using a scheme which guarantees stability before proceeding to the next time step (see Appendix A for details of the convection scheme). Once the density field is known, the stream function and the velocity field are updated as discussed above, and the procedure is repeated.

3. An Example Solution

In this section we present a description of the model output for one particular run. Wind stress is not included in this run, both for simplicity and to clarify its influence through comparison with later runs. A well-mixed surface layer, improved representation of the surface fields, the representation of the Indian Ocean and modified values of ε, K_V, and K_H are the primary differences from the results discussed by SW91*a*.

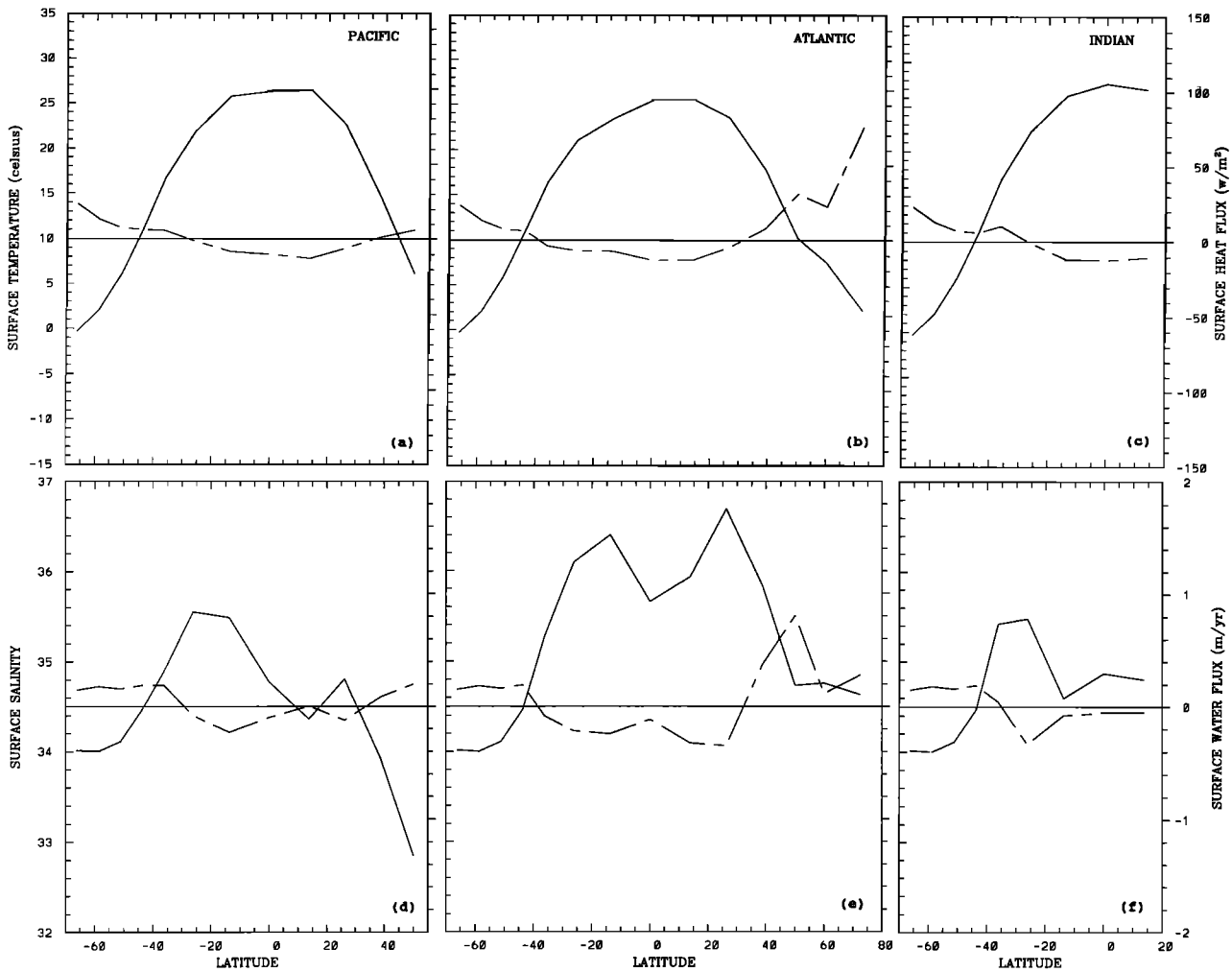

Fig. 2. Zonally averaged surface temperature and salinity for each of the ocean basins with a 50-day relaxation time for the upper 50 m (solid curves). Results south of 40°S correspond to our circumpolar Southern Ocean and are identical in each model region. Also shown are the model estimates of the surface heat flux and precipitation minus evaporation (broken curves).

All results presented in this paper were obtained after 5000 years of spin-up under restoring boundary conditions (13) and (14), with T^* and S^* given by the zonally averaged data of *Levitus* [1982] (Figure 2) and a restoring time scale of 50 days. The only remaining adjustable parameters are ε, K_V, and K_H. Results presented here correspond to values of $\varepsilon = 0.45$, $K_V = 0.44 \times 10^{-4}$ m^2 s^{-1} and $K_H = 10^3$ m^2 s^{-1}. The motivation for, and the model sensitivity to, these choices will be discussed in detail in the next section.

The geometry and the surface fields of temperature and salinity are substantially more realistic than those considered in SW91*a*, but the steady state solution predicted by the model is similar. The stream function (Figures 3*a*–3*c*) shows deep-water production only in the North Atlantic, at a rate of about 15 Sv (1 Sv = 10^6 m^3 s^{-1}). Only about 5 Sv of this water recirculates within the Atlantic, the remainder exiting into the Southern Ocean at depths exceeding 2000 m. Below 1000 m, deep water enters the Pacific Ocean at a rate of about 10 Sv, and the Indian Ocean at a rate of about 4 Sv. The water entering both Pacific and Indian oceans upwells roughly uniformly over the regions north of 40°S and returns to the Atlantic via the Southern Ocean as intermediate and upper water masses, qualitatively consistent with the conveyor belt circulation discussed by *Gordon* [1986]. Comparing with previous results presented in SW91*a*, *b* shows that the conveyor belt circulation is a robust feature of the ocean model under present-day forcing.

Zonally averaged temperatures and salinities are also illustrated in Figure 3, and the zonally averaged data of *Levitus* [1982] are reproduced in Figure 4 for comparison. The largest differences between model and observed results occur in the Southern Ocean and near the equator. The very cold, relatively saline Antarctic Bottom Water is not reproduced, and the upward bowing of isopycnals associated with equatorial upwelling is, of course, absent. The weakness of the Antarctic Bottom Water influence is also evident in the abyssal Pacific and Indian oceans, where conditions are too fresh.

The salinity field is significantly improved compared to that presented in SW91*a*, due primarily to the more accurate representation of the surface salinity used in the present study. In particular, the strong north-south asymmetry seen in the Pacific observations is now reproduced by the model. In addition, a salinity minimum is observed near the equator

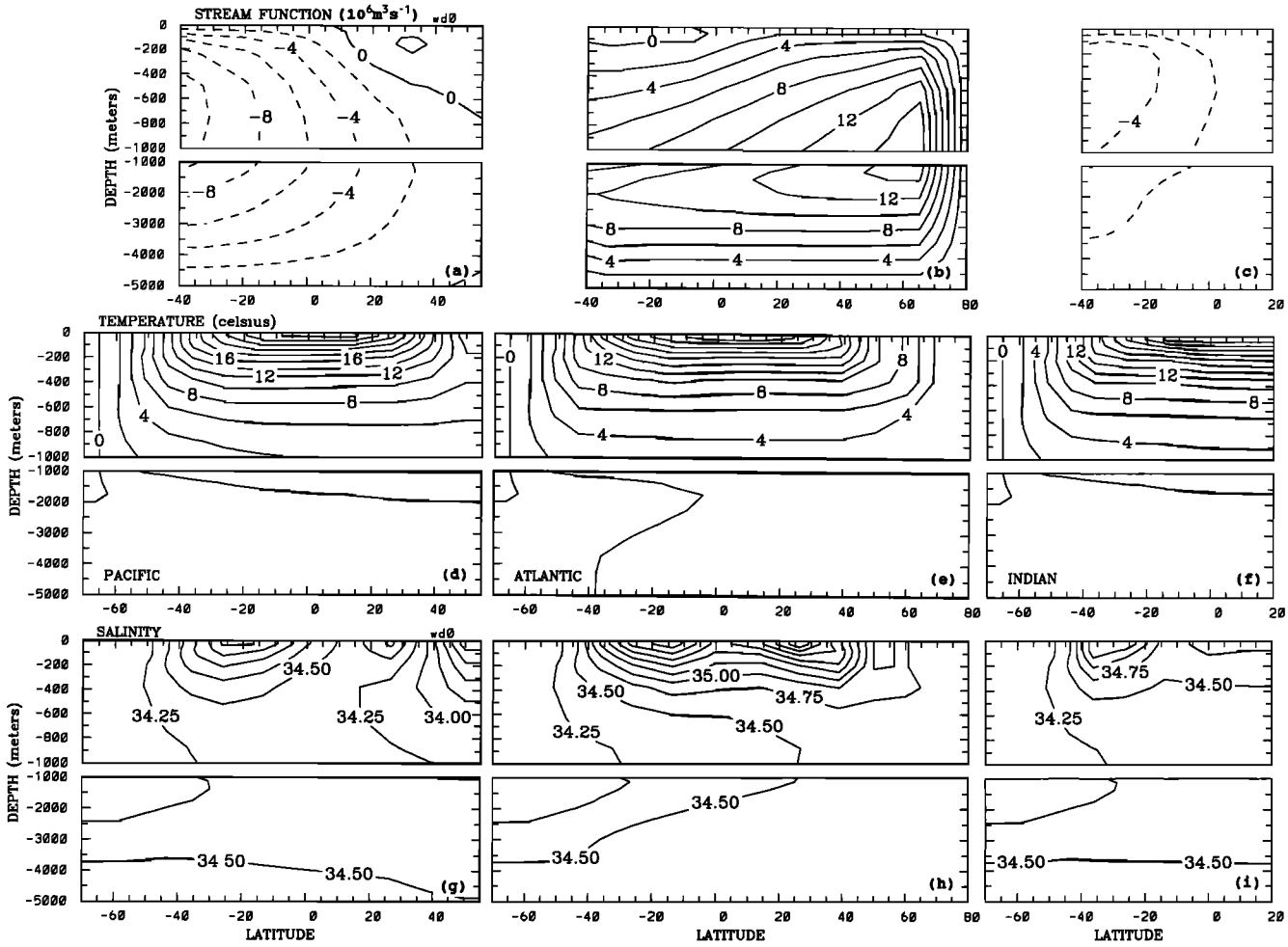

Fig. 3. The meridional (*a–c*) stream functions, (*d–f*) temperatures, and (*g–i*) salinities corresponding to the Pacific, Atlantic, and Indian Ocean regions of the model.

in the Atlantic, and the intrusion of relatively fresh Antarctic Intermediate Water into the Atlantic occurs higher in the water column and penetrates less far northward, giving a better representation of reality. However, the deep vertical penetration of relatively salty water is not seen at 35°N in the Atlantic, and the expected Antarctic Bottom Water influence in the South Atlantic is not evident.

The Indian Ocean was not included in SW91*a*. As for the other basins, the large-scale features of the temperature and salinity fields are reasonably reproduced, but again the absence of wind-driven equatorial upwelling and Antarctic Bottom Water is clearly apparent. In addition, the high salinities over the upper kilometer of the ocean north of the equator are not reproduced by the model. *Cox* [1989] indicates that a similar discrepancy seen in his OGCM results may be due to the absence of saline outflow from the Red Sea and the Persian Gulf. This possibility will be examined in section 6. It should also be noted that the very distinct subdomains of the Bay of Bengal (fresh) and the Arabian Sea (salty) are not resolved by our model.

The model estimates of the depth-integrated heat flux for each ocean basin are illustrated in Figures 5*a–5c*. In each case, the heat flux is highly asymmetric, heat being carried southward at most latitudes in the Pacific and Indian Oceans and northward in the Atlantic Ocean. The qualitative agreement with observational estimates is reasonable, but the heat fluxes estimated by the model are clearly too low.

The water fluxes are compared with observational estimates from *Baumgartner and Reichel* [1975] in Figures 5*d–5f*. For the purpose of this comparison, the *Baumgartner and Reichel* [1975] flux estimates have been plotted with the flux through the northern extreme of each basin set to zero, as is appropriate for comparison with the present run in which flow through the Bering Strait has been neglected. It is important to recognize that there are large uncertainties in these observational estimates, but they still represent a useful benchmark. There is some qualitative agreement between model and observational estimates, but the comparison is obviously poor.

Overall, the circulation and water mass properties predicted by the model compare favorably with the observations. Deep convection occurs primarily in the North Atlantic, a global conveyor belt of realistic strength is established, and the different character of the temperature and salinity structures observed in the three basins are reasonably reproduced. Differences between model and observational estimates of both heat and water fluxes are at least partially due to the absence of wind stress, as will be demonstrated in section 5.

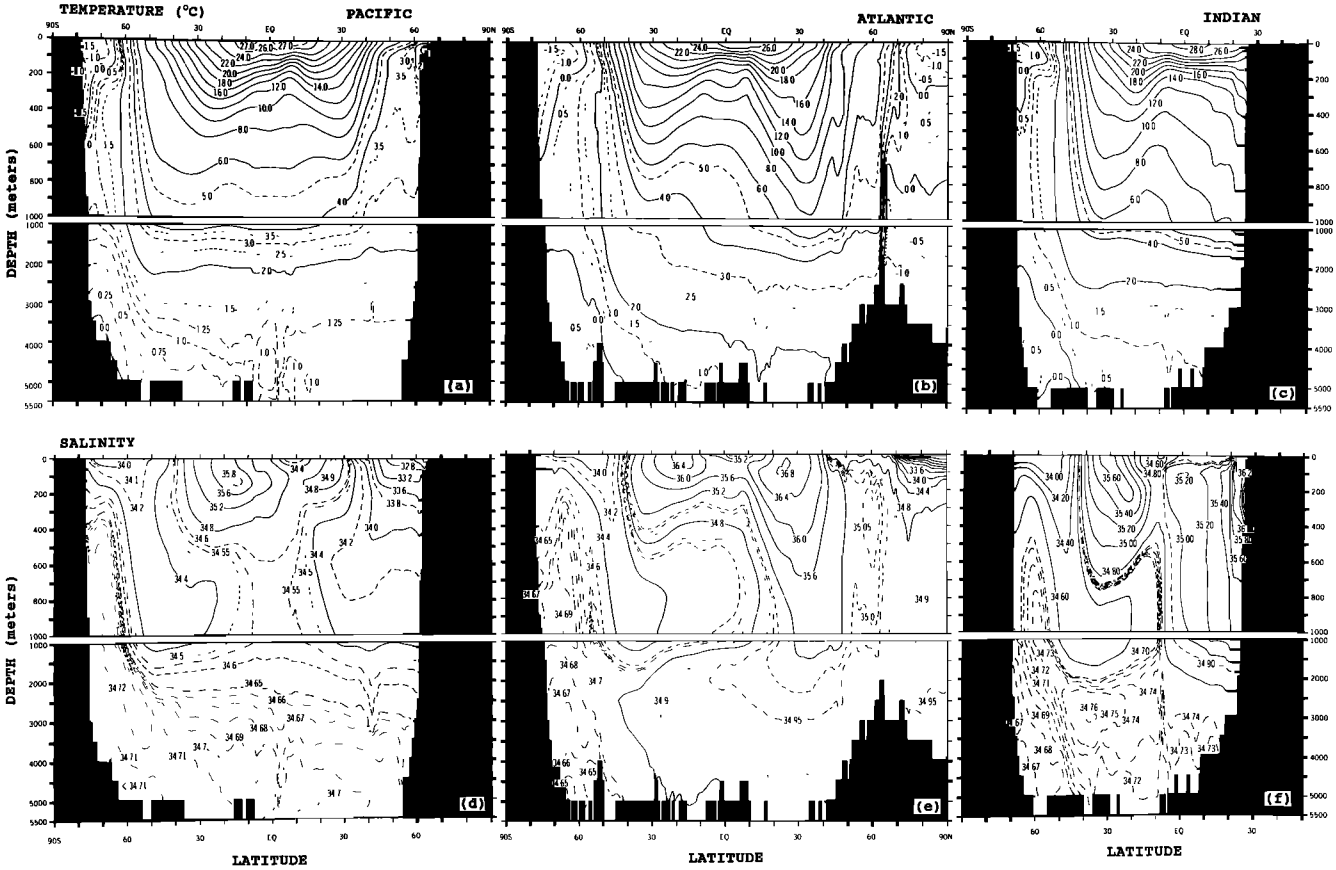

Fig. 4. Zonally averaged (*a–c*) temperature and (*d–f*) salinity fields in the Pacific, Atlantic, and Indian oceans from *Levitus* [1982].

4. Sensitivity to Model Parameters

In this section we consider the sensitivity of our model results to variations in ε, K_V, and K_H. Substantial uncertainties exist in the values for each of these parameters. Early work [e.g., *Munk*, 1966] indicated values of K_V of the order of 10^{-4} m^2 s^{-1}, but more recent direct estimates based on microstructure measurements [*Gregg*, 1987] indicate values of the order of 10^{-5} m^2 s^{-1}, at least in the thermocline away from boundaries. It seems likely that K_V increases with decreasing buoyancy frequency [*Gargett*, 1984], and this may have significant consequences [*Cummins et al.*, 1990]. However, only the simplest case of a constant value will be considered here. Comparison with OGCM results (WS91) suggests a value for ε of the order of 0.3–0.6, but since ε represents the influence of horizontal eddy stresses and other poorly defined processes, this range of values, based on comparison with a single OGCM experiment, should be considered as an optimistic indicator of the uncertainty in this parameter. Below, we take $K_V = 10^{-4}$ m^2 s^{-1} and $\varepsilon = 0.3$ as our standard values, and variations about these values are considered. Our standard value for $K_H = 10^3$ m^2 s^{-1} was chosen to be consistent with values used in previous OGCM studies [e.g., *Bryan and Lewis*, 1979; *Bryan*, 1987] and observational estimates [*Munk*, 1966; *Rooth and Ostlund*, 1972], but there is large uncertainty in this value also.

The dependence of OGCM results on K_V and K_H has been considered by *Bryan and Lewis* [1979] and *Bryan* [1987]. The parameter ε is unique to the zonally averaged model considered here, and sensitivity to variations of it have not been considered previously. The motivation for the form (9) given in WS91 indicates that ε is determined by the slight deviations of the zonally averaged flow from geostrophy. As such, it incorporates the influences of horizontal viscous and eddy stresses as well as damping by bottom stress. The corresponding surface stress is included separately through the specification of the surface Ekman flux.

Bryan [1987] gives a scale analysis of the equations, which provides a useful framework for the consideration of parameter variations. This analysis is briefly repeated here with the influence of wind stress omitted, but with ε included as a parameter.

The continuity equation (4) suggests $W \sim VD/L$, where L, $V(D, W)$ are horizontal (vertical) length and velocity scales. If the vertical structure of the density field is determined by a balance between advection and vertical diffusion, then

$$D = (K_V L/V)^{1/2} \tag{19}$$

and (3) with (10) and (11), suggest

$$V = \varepsilon g(\Delta\rho/\rho_*)D/(\Omega L) \tag{20}$$

Substituting (20) and (19) and rearranging terms, we obtain

$$D = \left(\frac{K_V \Omega L^2}{\varepsilon g(\Delta\rho/\rho_*)}\right)^{1/3} \tag{21}$$

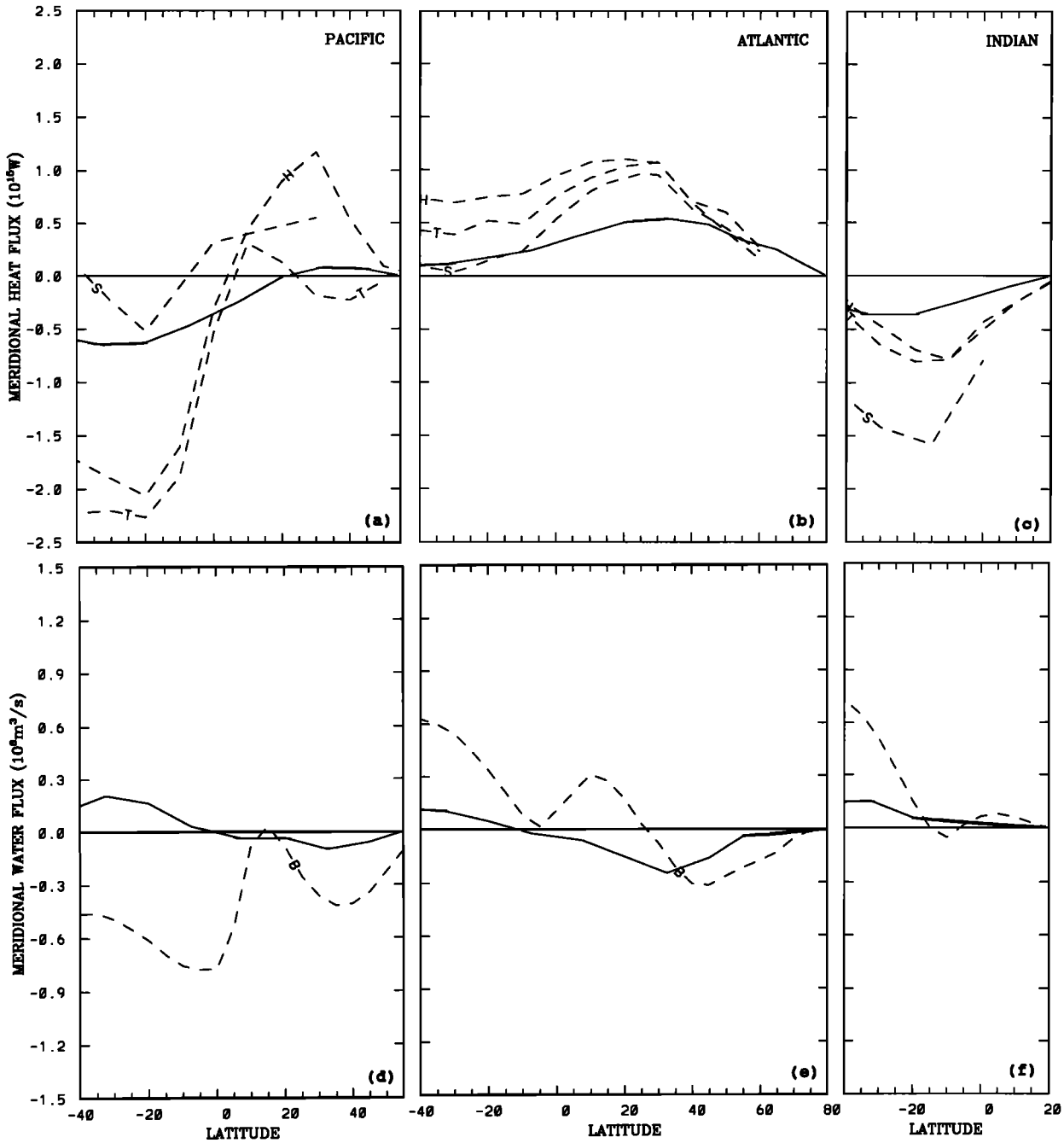

Fig. 5. (*a–c*) Model estimates of the depth-integrated heat flux for each of the ocean basins (solid curves). Also shown as broken curves are observational estimates taken from the literature (H, *Hastenrath* [1982]; T, *Talley* [1984]; *S*, *Hsiung* [1985]). (*d–f*) The model estimates of the depth-integrated water fluxes (solid curves), together with the observational estimates of *Baumgartner and Reichel* [1975] (dashed curves).

Finally, substituting (21) back into (20) gives

$$V = \left[\frac{\varepsilon g(\Delta\rho/\rho_*)}{\Omega}\right]^{2/3}\left[\frac{K_V}{L}\right]^{1/3} \tag{22}$$

and

$$\psi = VD = \left[\frac{\varepsilon g(\Delta\rho/\rho_*)K_V^2 L}{\Omega}\right]^{1/3} \tag{23}$$

where ψ is the scale for the meridional stream function.

It should be noted that within the downwelling region in the North Atlantic, advection, diffusion, and convection all act to carry the surface properties into the interior of the ocean, so the penetration of the surface density is not determined by a balance between advection and diffusion in the straightforward way implied by (19). However, the density in this downwelling region is essentially depth independent, and it tends to determine the density throughout the deep ocean to the south. Thus, the depth penetration of the surface properties in the column immediately to the

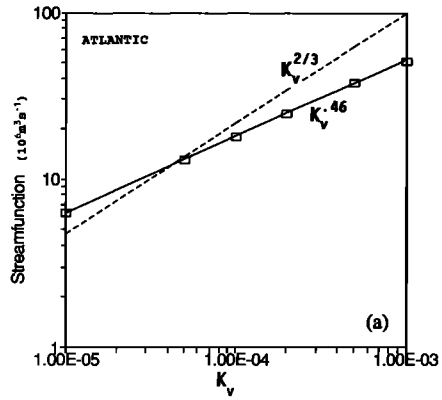

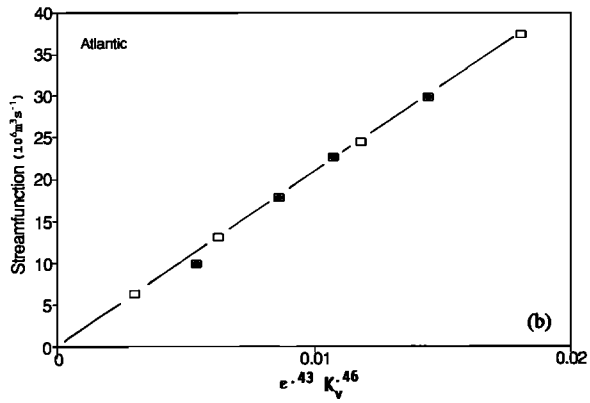

Fig. 6. (*a*) The maximum value of the stream function in the Atlantic basin plotted against K_V on log-log axes. The two straight lines correspond to $K_V^{0.46}$ and $K_V^{2/3}$ dependence. (*b*) The maximum value of the Atlantic stream function plotted against $\varepsilon^{0.43} K_V^{0.46}$. Results with K_V fixed and ε varying are indicated by open squares and those with ε fixed and K_V varying are indicated by boxed crosses.

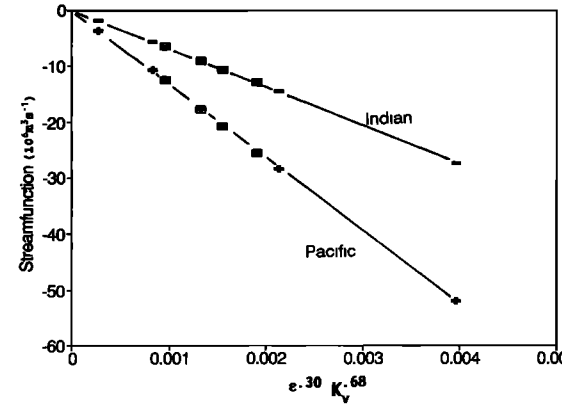

Fig. 7. The maximum value of the stream function in the Pacific and Indian Ocean basins plotted against $\varepsilon^{0.30} K_V^{0.68}$. Results are shown for ε fixed and K_V varying and for K_V fixed and ε varying. The latter are indicated by boxed crosses.

south of the downwelling region determines the penetration depth of the surface density difference, and the parameter dependencies determined by the above scale analysis should hold even in this region.

Equation (23) suggests that the overturning stream function should scale like $K_V^{2/3}$. Figure 6*a* shows a log-log plot of the maximum value of the overturning stream function in the Atlantic basin plotted against K_V. Clearly, ψ is very nearly proportional to $K_V^{0.46}$ rather than $K_V^{2/3}$. When a similar plot is produced with wind forcing included, the dependence reduces further to $K_V^{0.36}$ for values of K_V greater than 5×10^{-5} m^2 s^{-1} (for smaller values of K_V the surface Ekman cells carry the largest transport, and the above scaling is entirely inappropriate). Based on results from an OGCM, *Bryan* [1987] obtains a similar result with ψ proportional to $K_V^{1/3}$ (with wind stress included) rather than $K_V^{2/3}$, and notes that no explanation for this dependence has been presented. One might expect reduced sensitivity to K_V in this basin as a simple consequence of the presence of deep convection, which represents an additional vertical mixing process not included in the above scaling argument. Indeed, when the corresponding plot is constructed for the other basins in our model, where convection is weak or absent, it is found that ψ is very nearly proportional to $K_V^{2/3}$, as suggested by (23) (see Figure 7). However, additional model runs with a single basin geometry show that reduced sensitivity to K_V does not always occur in the vicinity of convective regions. Thus, while reduced sensitivity to K_V in the Atlantic is consistent with the presence of deep convection in this region, the details of how convection affects the maximum overturning rate are still not well understood.

Figures 6*b* and 7 illustrate the maximum overturning stream function as a function of ε and K_V for the different ocean basins. Each plot shows results for K_V varying between 10^{-5} and 2×10^{-4} m^2 s^{-1} with all other parameters held fixed, as well as results for ε varying between 0.1 and 1.0 with all other parameters fixed. Equation (23) gives a good estimate of the sensitivity to these parameters in both the Pacific and Indian basins. While power law dependencies also hold in the Atlantic basin, the exponents are poorly approximated by the simple scale analysis.

Finally, we note that the diapycnal mixing in our model also includes the implicit diffusivity $K_I = K_H m^2$ caused by the horizontal diffusivity acting across isopycnal surfaces of slope m, which *Cummins et al.* [1990] have shown may actually be larger than the explicit diffusivity K_V. Since this effect contributes to diapycnal mixing, it may also contribute to the reduced sensitivity to K_V discussed above. To examine the significance of this effect, the results shown in Figure 6 were reproduced with $K_H = 0$; there is no significant change in the K_V dependence. This may seem somewhat surprising in light of *Cummins et al.*'s [1990] results, but for these buoyancy-driven runs, large isopycnal slopes are associated with regions where convection dominates over diffusive diapycnal mixing. Also, by considering zonally averaged equations, we have reduced the effective value of m across which horizontal diffusion acts so diapycnal mixing will be correspondingly reduced (e.g., the Gulf Stream recirculation region has large values of m associated with it which are totally absent from our model).

Figure 8 illustrates the sensitivity of the stream function in each basin to changes in K_H. As K_H increases, the horizontal density gradients are reduced at depth, and hence the model currents are also reduced. However, the dependence of ψ on K_H is rather weak.

Since the present model has been developed for the purpose of studying climate dynamics, it is of particular interest to consider the sensitivity of the model heat and

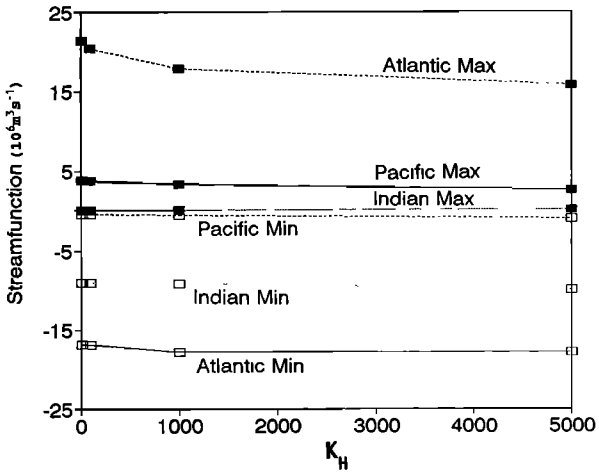

Fig. 8. The maximum and minimum values of the stream function in each ocean basin as functions of K_H.

water fluxes to parameter variations. The model heat fluxes are illustrated for different values of K_V, K_H, and ε in Figure 9. K_V varies from 10^{-5} to 2×10^{-4} m^2 s^{-1}, K_H varies from 10^2 to 5×10^3 m^2 s^{-1}, and ε varies from 0.1 to 1.0. It should be stressed that these parameter ranges were chosen to illustrate extreme values.

Variations in K_V, K_H, and ε have similar influences on the heat fluxes in the Pacific and Indian oceans. In each case, the amplitude of the fluxes increases as the parameters increase, but there are no qualitative changes in the nature of the fluxes. In the Atlantic Ocean, both K_H and ε have an additional influence: either decreasing K_H or increasing ε results in a greater tendency for the heat flux to be positive in the southern hemisphere. These changes are of considerable interest, since *Wunsch* [1984] finds that a positive heat flux at all latitudes within the Atlantic is a robust feature of his diagnostic study, setting an important constraint on our model.

Finally, we note that the results are substantially more sensitive to variations in K_V and ε than to variations in K_H. If one restricts attention to the small range of ε suggested by the comparison with OGCM results (0.3–0.6), then K_V is the source of greatest uncertainty. However, it should be remembered that this range of ε values is based on one particular model run of an OGCM and hence represents an optimistic estimate of the uncertainty in this quantity. The fact that the heat flux can be changed by a factor of 2 through quite reasonable changes in K_V emphasizes the need to better understand diapycnal mixing in the ocean. On the other hand, the variations with all three parameters are smooth, so we are encouraged that useful work can be done with the estimates presently available.

Figure 10 illustrates the sensitivity of the model estimate of water flux to variations in K_V, K_H, and ε. Variations in K_V and ε again substantially modify the amplitude of the fluxes but do not change the qualitative structure. Increasing K_H increases the flux magnitudes within the Pacific and Indian basins, while in the Atlantic, it increases the northward flux at nearly all latitudes. However, results are relatively insensitive to variations in K_H if we restrict attention to values less than 10^3 m^2 s^{-1}.

Several additional model runs were done to examine the effect that numerical diffusion would have on our solutions if a simple upwind differencing scheme had been used. Results show little influence on either the ocean circulation or the temperature and salinity fields. The largest effect is seen in the surface and integrated meridional flux estimates, particularly the water flux estimates. Examples of the influence are shown in Figures 9 and 10. In the plots with K_V (K_H) varying, the curves indicated by "diff" in the key show the influence of vertical (horizontal) numerical diffusion in isolation. In the plots with ε varying, the curves indicated by "diff" include both horizontal and vertical numerical diffusion. Quantitative estimates based on (18) show that both horizontal and vertical numerical diffusion exceed the corresponding explicit coefficients in the vicinity of the deep convection occurring in the North Atlantic. The impact is presumably reduced by the fact that the influences of advection and convection are dominant in this area. In fact, the results presented in this section would not be significantly altered if numerical diffusion had not been accounted for at all. However, as we shall discuss in the next section, this effect becomes more significant with the inclusion of wind stress.

The sensitivity results presented above could now be used to suggest improved estimates of the values of K_V and ε. In particular, according to (21) the vertical scale (away from the convection region) can be reduced by a factor γ by simply reducing $(K_V/\varepsilon)^{1/3}$ by γ. Similarly, we may modify the rate of production of deep water in the North Atlantic by the factor δ by changing $\varepsilon^{0.43} K_V^{0.46}$ by this factor. These two conditions are satisfied simultaneously by changing K_V by the factor $\delta^{1.12}\gamma^{1.45}$ and ε by the factor $\delta^{1.12}\gamma^{-1.55}$.

In this section we have used base values of $K_V = 10^{-4}$ m^2 s^{-1} and $\varepsilon = 0.3$. The values of $K_V = 0.44 \times 10^{-4}$ m^2 s^{-1} and $\varepsilon = 0.45$, used in Figure 3 and throughout the remainder of this paper, correspond to $\gamma = 0.66$ and $\delta = 0.82$, so that the depths of the thermocline and the core of the Antarctic Intermediate Water are reduced by about 33%, and the maximum value of the stream function is reduced by about 18% (from 18 to 15 Sv) in the Atlantic and by about 35% in both the Pacific and Indian oceans.

The differences between our base values and our final values of ε and K_V are acceptable when compared with the uncertainty in these parameters, and the reduction in K_V is consistent with suggestions from recent direct estimations based on microstructure measurements. The main difference between the water mass properties based on the two different sets of parameters is the depths of the intrusions of Intermediate Waters mentioned above. However, the changes in circulation and water mass properties combine to result in a decrease in the magnitude of the heat flux by about 40% in the Pacific and Indian oceans, and a decrease by about 20% in the Atlantic Ocean (compare the solid curves in Figure 9 with the model estimates shown in Figure 5). Thus the values of K_V and ε used in section 3 result in improved representation of the water mass properties at the expense of a degradation of the estimated meridional heat and water fluxes. It might certainly be argued that for the purpose of climate modeling this trade-off is not acceptable. However, as we shall see below, other factors are important in determining the horizontal heat and water fluxes.

5. Wind Stress

Figure 11 illustrates the meridional stream function, temperature, and salinity with the influence of a mean wind

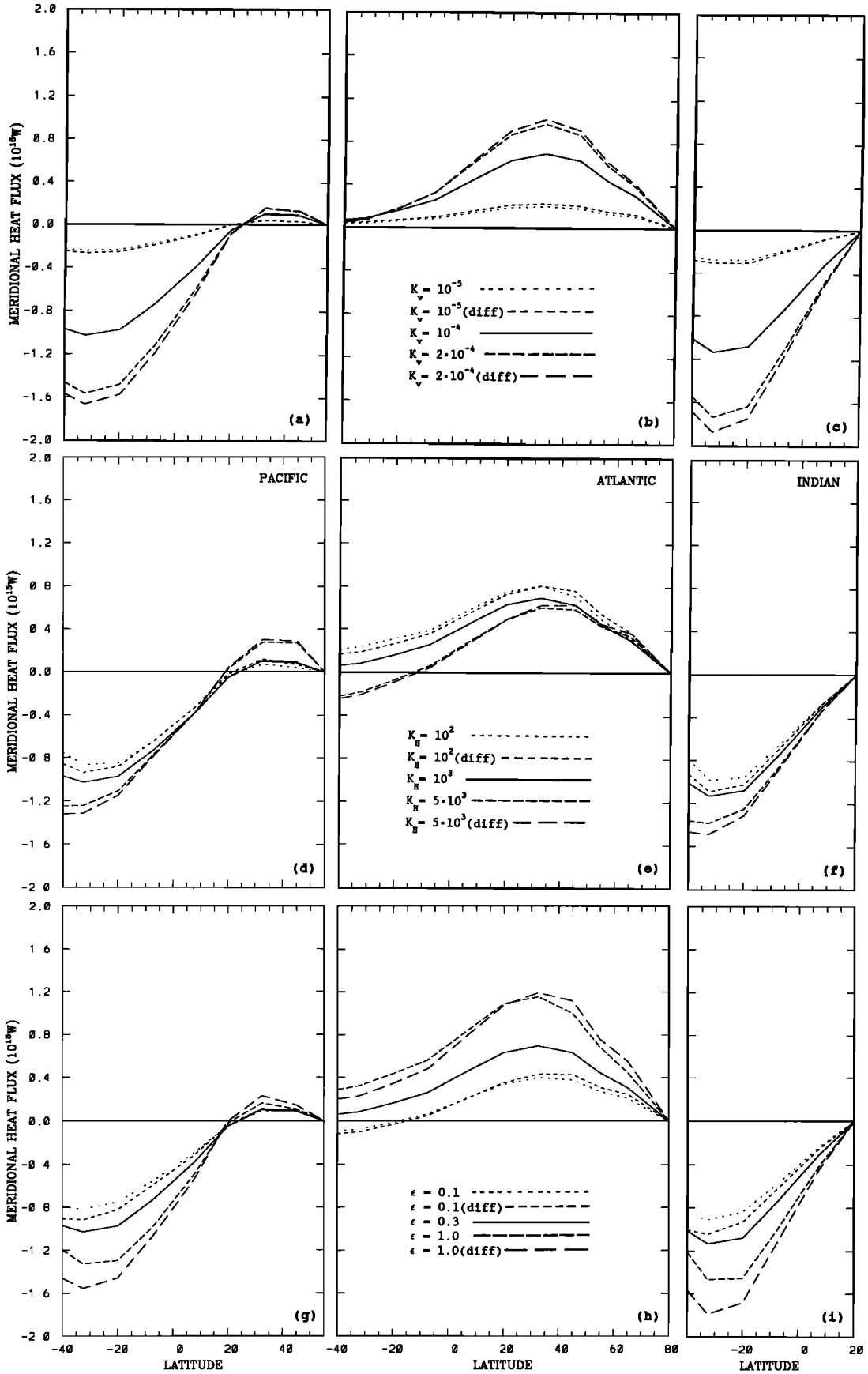

Fig. 9. The depth-integrated meridional heat flux within each ocean basin for (*a–c*) several values of K_V, (*d–f*) several values of K_H, and (*g–i*) several values of ε. The symbol "diff" in the key indicates that numerical diffusion has not been suppressed. Fluxes for the Indian Ocean have been multiplied by 2 to reduce crowding. Diffusion coefficients are in square meters per second.

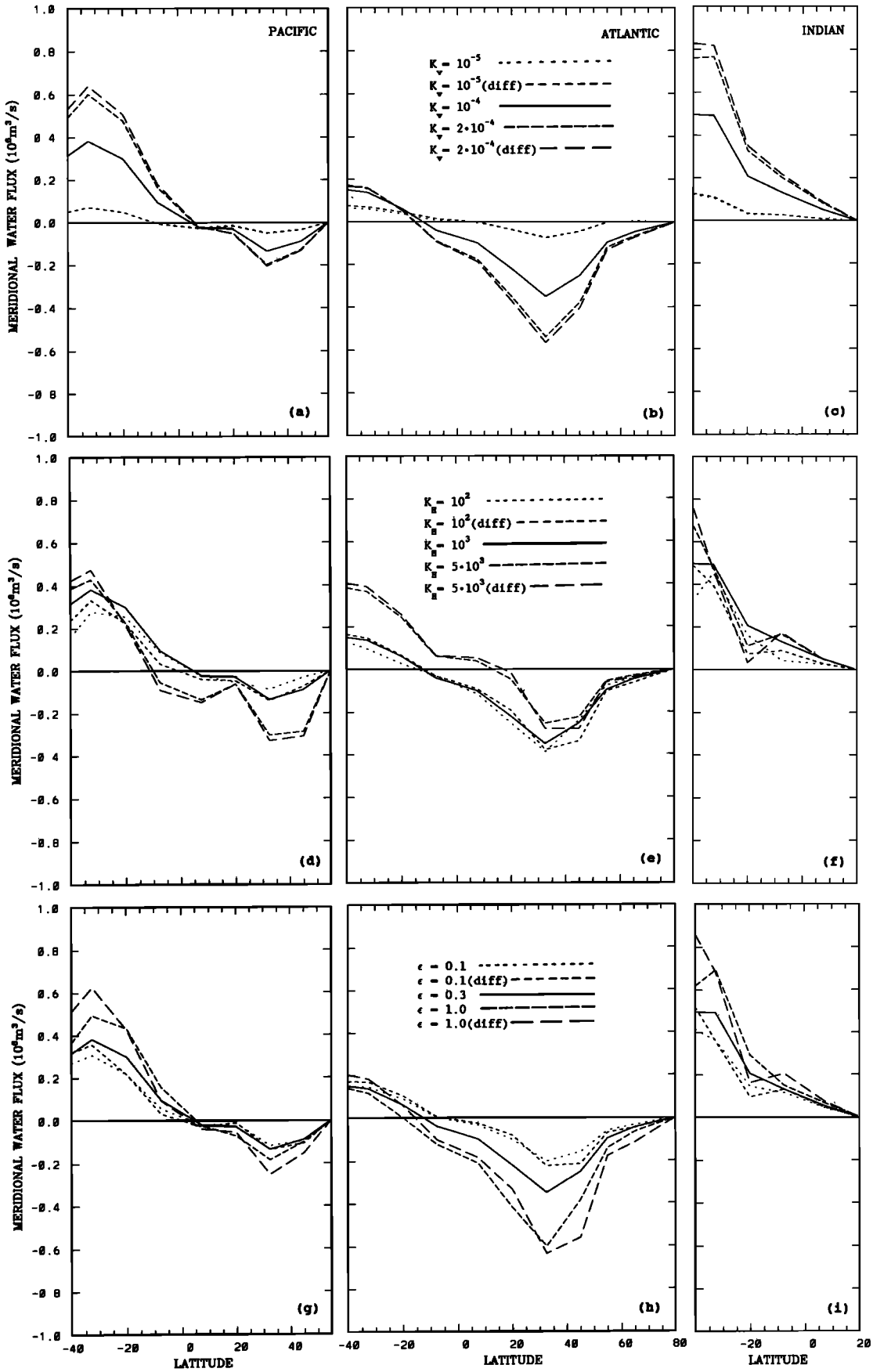

Fig. 10. The depth-integrated meridional water flux within each ocean basin for (*a–c*) several values of K_V, (*d–f*) several values of K_H, and (*g–i*) several values of ε. The symbol "diff" in the key indicates that numerical diffusion has not been suppressed. Fluxes for the Indian Ocean have been multiplied by 2 to reduce crowding. Diffusion coefficients are in square meters per second.

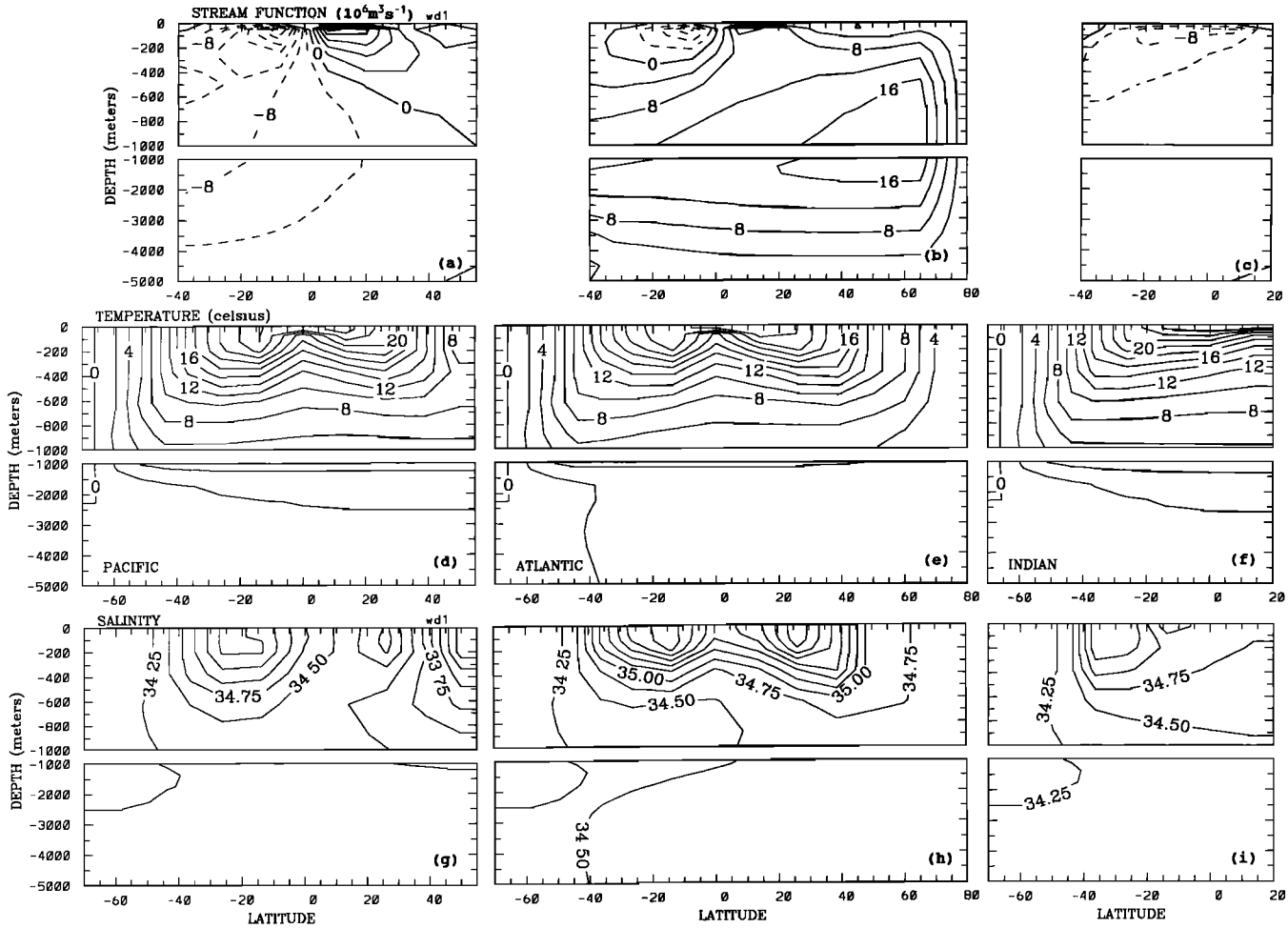

Fig. 11. As in Figure 3 but including the influence of zonal wind stress forcing estimated from *Han and Lee* [1983].

stress as given by *Han and Lee* [1983] included. Changes in the stream function relative to Figure 3 (no wind stress) are seen in the upper kilometer of each ocean basin, particularly near the equator, where the Ekman fluxes are largest. Indeed, the largest transports are now associated with the Ekman fluxes, with the maximum value reaching 33 Sv in the Pacific Ocean at the first cell boundary south of the equator (7°S). The limited penetration depth of the Ekman cells is consistent with results of OGCMs [e.g., *Bryan and Lewis*, 1979] and at least crudely with the advective depth scale of *Bryan* [1987]. As expected, the model now reproduces the observed upward bowing of isotherms near the equator. Changes in the salinity field are relatively small. Figure 12 shows the model estimates of the depth-integrated heat and water fluxes with the influence of wind stress included. The heat flux estimates of *Talley* [1984] and water flux estimates based on *Baumgartner and Reichel* [1975] are included for comparison, but recall that there is considerable uncertainty in these values (e.g., see Figure 5). The solid lines indicate the basic model results. Wind stress clearly results in much better agreement between our model heat flux estimates (Figures 12*a*–12*c*) and the observational estimates. The magnitude of the heat flux is increased in each basin, and the large gradients observed near the equator are now reproduced by the model. In spite of the strong southward Ekman flux just south of the equator, the heat flux remains northward at all latitudes in the Atlantic basin.

It should be noted that the larger heat fluxes obtained with wind stress could be achieved without including this effect simply by adjusting K_V and/or ε. Including wind stress is the preferred approach primarily because it is a real effect that should be accounted for. Also, increasing the heat fluxes by adjusting K_V and ε would be accompanied by changes in the temperature and salinity fields: increasing K_V will deepen the thermocline and the depth of salinity features, and increasing ε will have the opposite effect. In both cases, the deep overturning circulation will be increased to carry the additional flux.

Results for the water fluxes (solid lines in Figures 12*d*–12*f*) still compare rather poorly with the observational estimates. Interestingly, preliminary results obtained using a numerical scheme which did not attempt to reduce the influence of numerical diffusion actually showed better agreement with the *Baumgartner and Reichel* [1975] observational estimates. This is not too surprising, since in reality, one might anticipate enhanced horizontal diffusion in regions of larger horizontal velocities, and this is what the numerical diffusion associated with a simple upwind differencing scheme gives (see (18)), albeit in an uncomfortably, uncontrolled manner.

To clarify the effect of horizontal diffusion of this nature,

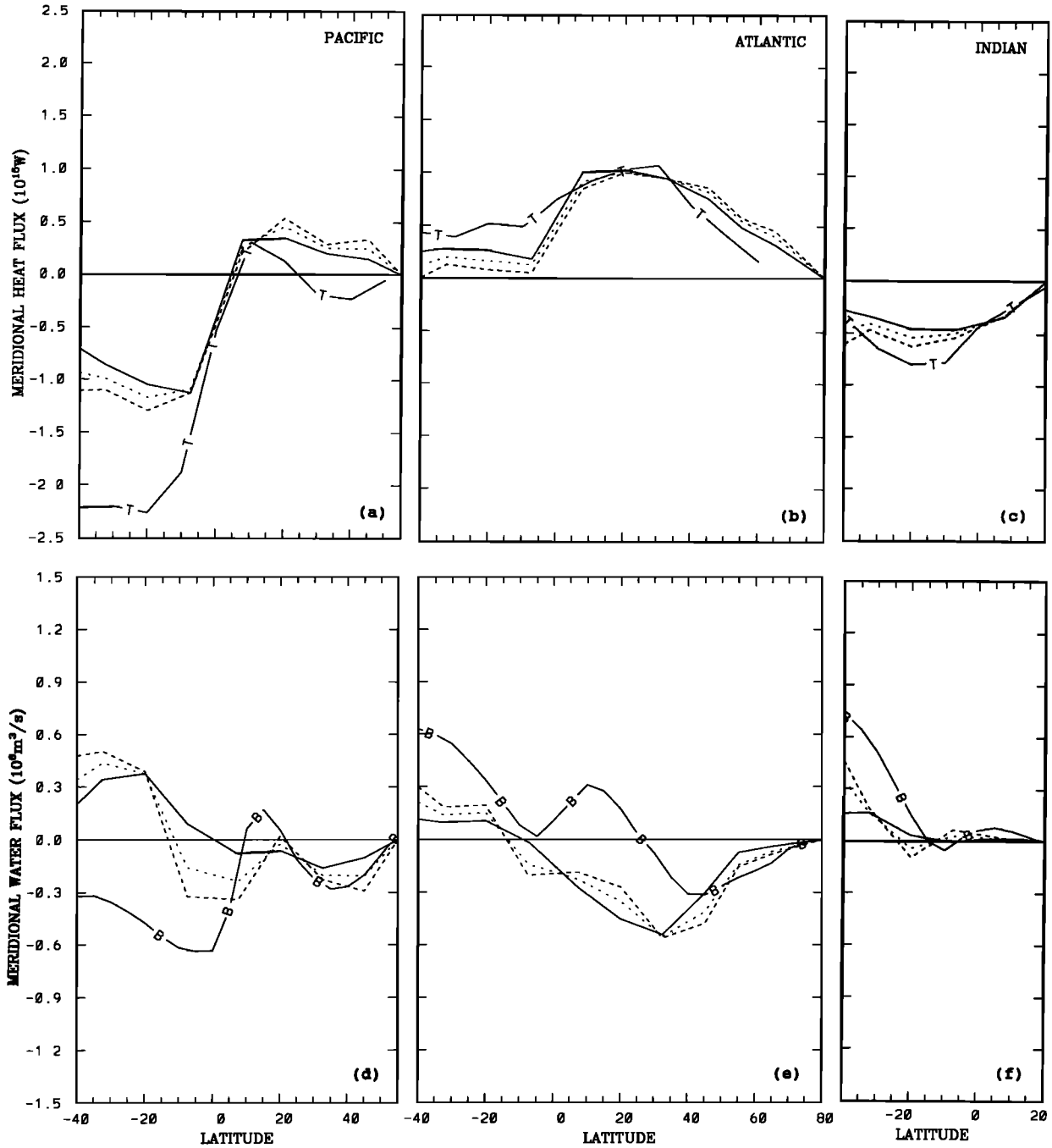

Fig. 12. As in Figure 5 but with the influence of wind stress included. The three curves on each plot correspond to $K_H = 10^3$ m^2 s^{-1} + $va\Delta\phi$ with $\Delta\phi = 0°$ (solid curves), 5° (dotted curves), and 10° (dashed curves). *Talley*'s [1984] heat flux estimates and *Baumgartner and Reichel*'s [1975] water flux estimates are shown for comparison.

two additional runs were performed with horizontal diffusion increased by an amount proportional to the local north-south current speed. That is, results were determined for $K_H = 10^3$ m^2 s^{-1} + $va\Delta\phi$, where $\Delta\phi$ is a constant. The broken lines in Figure 12 correspond to $\Delta\phi$ values of 0.087 (5°, short dashes) and 0.17 (10°, long dashes). The influence is largest for the water flux estimates due to the relatively small scales imposed on the salinity through the surface boundary condition. Clearly, the inclusion of explicit diffusion of this form improves the correspondence of the water fluxes with the observational estimates for the spatial variations on scales of the order of 20°. It is also clear that one could choose $\Delta\phi$ to be a function of position, which would further improve the results. This will not be done here, but all runs shown below will include the adjustment in K_H described above with $\Delta\phi = 0.17$. The larger scales are not significantly affected by the additional horizontal diffusion. In particular, the results for the South Pacific still show large differences from the observational estimates. While the differences are most likely due to model deficiencies, it is perhaps worth recalling that the observational estimates are most uncertain in this region, with possible errors as large as the differences between model and observational estimates seen in Figure 12 [*Baumgartner and Reichel*, 1975; *Wijffels et al.*, 1992].

Finally, it is important to realize that the changes in stream function, temperature, and salinity associated with the change in K_H described above are relatively small. The changes in K_H are largest in the top layer of the model and insignificant below a few hundred meters depth. The associated changes in the horizontal fluxes are largely compensated by modifications in the surface fluxes of heat and salt. Thus changing K_H near the surface has little influence on either circulation or watermass properties, but it does significantly influence the surface fluxes of heat and (especially) water.

6. Interbasin Exchanges

The Mediterranean and Red Sea Influences

Both observations and theory show that there is exchange between the Atlantic Ocean and the Mediterranean Sea at a rate of the order of 1 Sv [*Lacombe and Richez*, 1982; *Bryden and Stommel*, 1984] and exchange between the Indian Ocean and the Red Sea at a rate of the order of 0.33 Sv [*Siedler*, 1968, 1969]. Similar exchange must also occur between the Indian Ocean and the Persian Gulf, but we are not aware of any studies of this exchange. In each case, relatively fresh water enters the adjoining marginal sea near the surface, and relatively saline water exits below. Zonal sections suggest that the exiting water penetrates into the Atlantic to a depth of the order of 1000 m and into the Indian Ocean to a depth of the order of 500 m. These exchanges effectively extract heat and salt from the surface layer and replace it at depth, with subsequent redistribution by advection and diffusion. It is believed that this vertical exchange is the primary cause of the salinity maximum around 35°N in the Atlantic Ocean (Figure 4*e*) and north of the equator in the Indian Ocean (Figure 4*f*). Neither of these salinity features are reproduced in the runs above. The purpose of this section is to test whether accounting for the vertical exchange associated with these marginal seas is sufficient to remove these discrepancies with observations.

We have modified the model to include extraction of heat and salt from the surface layer of the Atlantic Ocean between 32.5° and 40°N at a rate corresponding to a volume flux of 1 Sv, and from the surface layer of the Indian Ocean between 7° and 20°N at a rate corresponding to a 0.45 Sv volume flux (0.33 Sv for the Red Sea and 0.12 Sv to roughly account for the Persian Gulf). All of the heat and salt carried by these waters is returned to the same latitude bands in the two model cells between 500 and 1000 m in the Atlantic and in the two cells between 250 and 750 m in the Indian Ocean. In each case, according to the studies quoted above, approximately 10% of the water volume extracted from the surface layer is lost due to an excess of evaporation over precipitation in the adjoining marginal seas. The circulation is thus completed by upwelling back to the surface layer at rates corresponding to 90% of the original volume fluxes. (The remaining 10% of the volume flux must, in reality, be compensated by depth-integrated flow, which is not explicitly included here due to the rigid lid approximation. Further discussion of this point is given in the next subsection.) Since the net salt flux into the marginal seas vanishes, the vertical exchange of salt should be correct, but any heat gained within these regions is neglected. Both the latitude bands and the depth ranges immediately influenced by the marginal seas are rather crudely specified. They could easily be changed, but this is unnecessary for the present purpose. We emphasize that our intention is not to perform a detailed fit, but to see if the effect of this kind of vertical exchange is of the correct order.

To obtain a more accurate representation of the Indian Ocean in the region directly influenced by exchange with the Red Sea, one additional change was made. The angular width of the Indian Ocean was reduced to 45° in the equatorial grid cell and to 35° north of 7°N.

A run with the Mediterranean and Red Sea influences included as described above showed local improvements in the temperature and salinity fields, as will be discussed below. However, the deep salinities in the Southern Ocean and in the Pacific and Indian basins were still much too fresh, similar to the results shown in Figure 11. The addition of a meridional ridge across the Southern Ocean as described in Appendix B made these deep salinities even fresher due to the increased input of fresh waters from around Antarctica. From a comparison of results with Figure 4, we note that our model estimates of the deep salinities around Antarctica are much too fresh (compare Figure 4 with Figure 11). Further, Figure 4 suggests that the relatively saline deep water around Antarctica plays an important role in maintaining the higher salinities observed in the deep basins to the north. These high salinities result from salt rejection during ice formation, an effect which is not included in our model. To test the effect that higher salinities in the southernmost cell would have on the remainder of the global ocean, two changes were made. First, as mentioned already, a meridional ridge at depths below 2500 m was added in the Southern Ocean in order to allow a deep, geostrophically balanced meridional circulation at the highest southern latitudes (see Appendix B for details). Second, the relaxation value for the surface salinity in the southernmost cell was increased from 34.0 to 34.7 to be more representative of conditions during deep-water formation.

Figure 13 shows the stream function, temperature, and salinity fields with the Mediterranean, Red Sea, and Southern Ocean influences included as discussed above; otherwise the model setup is exactly as for Figure 11. Compared with Figure 11, the largest change in the stream function occurs in the Atlantic, where the maximum value is reduced. Additional experiments show that this change is primarily due to the increased surface salinity specified in the Southern Ocean. As expected, both temperature and salinity are increased beneath a band centered on 35°N in the Atlantic Ocean, resulting in better agreement with the observations shown in Figure 4. The largest changes are in the salinity field: the 35 contour now extends below 2000 m in the North Atlantic compared to 350 m at the corresponding latitude in the South Atlantic. Although these results are preliminary, they clearly lend support to the idea that the deep penetration of salt visible in the zonal average below 35°N in the Atlantic is due primarily to the Mediterranean influence.

The influence of the Red Sea (and Persian Gulf) on the Indian Ocean is also significant. Both temperatures and salinities are increased north of the equator, the maximum salinity now exceeding 35.5. Isotherms are pushed down and salinity tends to be more vertically uniform above 1000 m. These changes result in substantially better agreement with the observations presented in Figure 4.

The increased surface salinity in the southernmost cell of

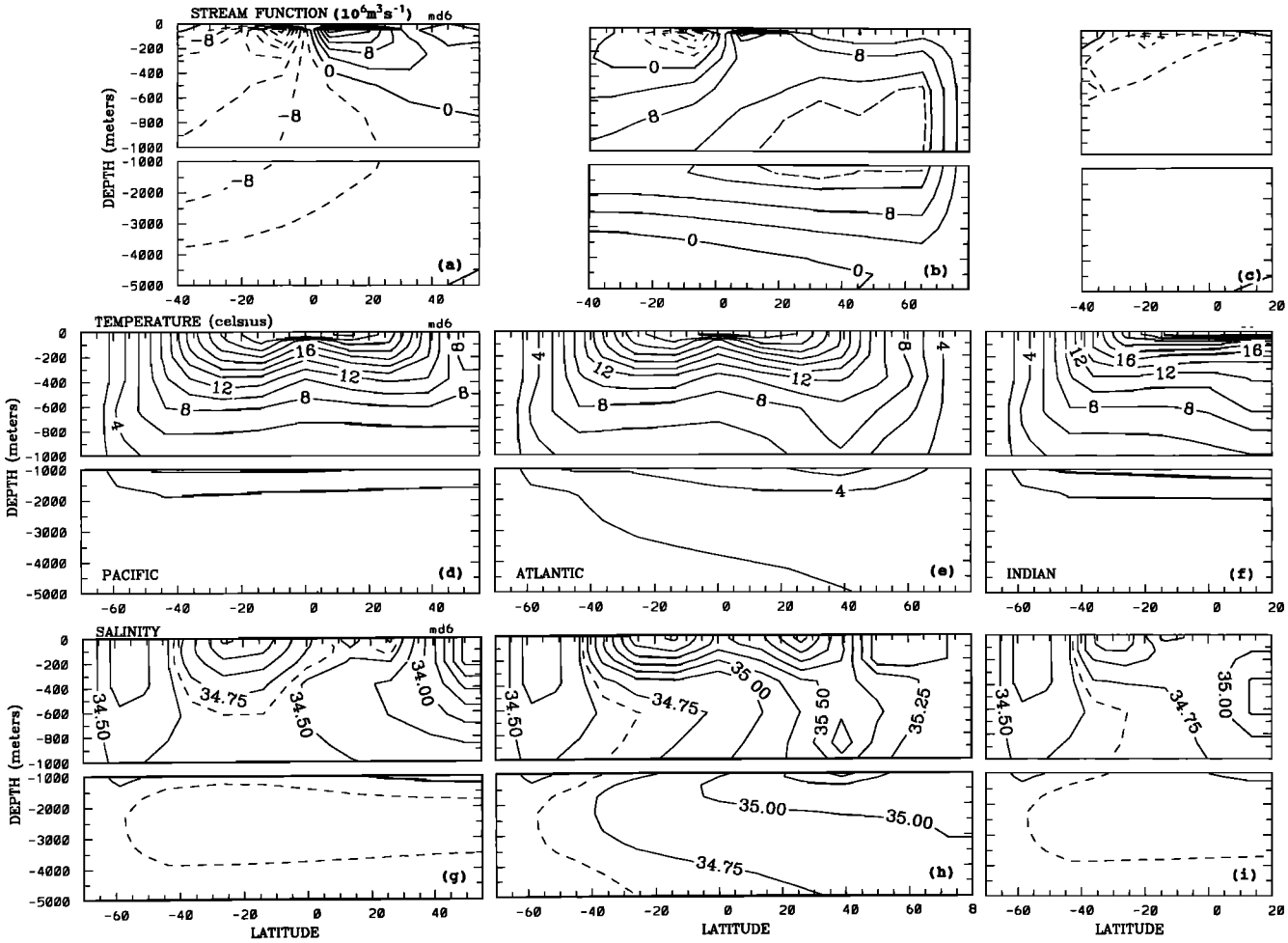

Fig. 13. As in Figure 3 but with the influences of wind stress forcing, exchanges with the Mediterranean and Red seas, and increased surface salinities around Antarctica all included, as discussed in the text. (*b*) The 14-Sv contour has been added as a broken line, and (*g–i*) the 34.6 contour has been added.

the Southern Ocean has resulted in increases in the deep salinities throughout the global ocean by nearly 0.2 compared to a run with the Mediterranean and Red Sea influences included but no modifications in the Southern Ocean. In addition, it has resulted in a deep overturning cell in the Atlantic basin which carries Antarctic Bottom Water into this basin. A further increase in the surface salinity of the southern surface cell could improve the results further, but this tuning exercise will not be pursued here. The important point to note is that to improve the deep salinities in the global ocean, the treatment of high-latitude processes must be improved.

Figure 14 illustrates the meridional heat and water fluxes for several model runs. Each of the flux estimates were determined by setting the flux to zero at the northern extreme of each basin and determining latitudinal variations from the integrated surface flux, this allows direct comparison with the corresponding observational estimates based on bulk aerodynamic formulae. The solid curve corresponds to Figure 3 without wind stress, and the line of shortest dashes corresponds to Figure 11 with wind stress. Of the various effects considered here, the influence of wind stress is the most significant. The effect of the marginal seas is indicated by the line with the next shortest dashes. It is interesting that the inclusion of the marginal seas gives more realistic regional temperature and salinity distributions, but has little effect on the larger scale heat and water fluxes. This leads us to suggest that exclusion of the explicit influence of these effects from our model will not substantially degrade its usefulness for climate studies. It should be emphasized, however, that we do not claim that the Mediterranean and Red seas have insignificant influence on the ocean circulation. All results shown in Figure 14 were determined under relaxation boundary conditions, and hence all the results are influenced by the adjoining marginal seas through the observed surface temperature and salinity fields with which the model is forced.

The last two curves shown in Figure 14 indicate the influence of exchange through the Bering Strait and the Indonesian passages and will be discussed below.

Flow Through Bering Strait and the Indonesian Passages

Recently, *Coachman and Aagaard* [1988] and *Aagaard and Carmack* [1989] have shown that about 0.8 Sv of relatively fresh water flows through the Bering Strait. There have also been several studies of the flow through the Indonesian passages, and volume flux estimates range be-

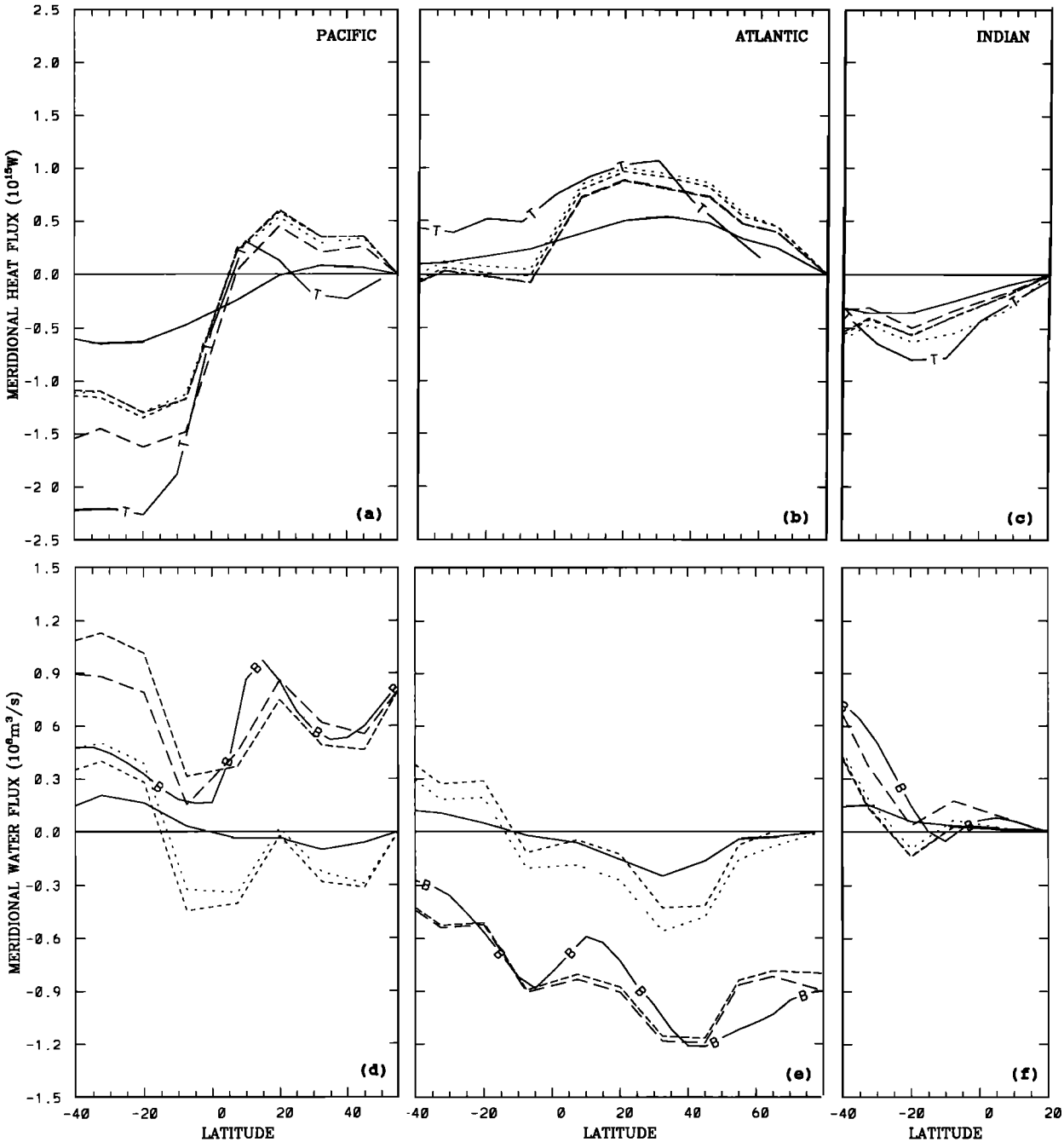

Fig. 14. The solid curve corresponds precisely to Figure 5. The broken curves include additional effects with the dashed segments increasing in length with the inclusion of more effects. Effects considered are wind stress, exchanges with the Mediterranean and Red seas, exchange through the Bering Strait (0.8 Sv), and exchange through the Indonesian Passages (20 Sv). The final curve also includes an explicit addition of fresh water to the Arctic Basin. *Talley*'s [1984] heat flux estimates and *Baumgartner and Reichel*'s [1975] water flux estimates are shown for comparison.

tween 1 and 20 Sv [*Gordon*, 1986], the more recent estimates [e.g., *Fieux et al.*, 1991] favoring the larger value. *Godfrey and Golding* [1981] and *Wijffels et al.* [1992] emphasize the possible significance of these exchanges in determining the large-scale watermass properties and ocean circulation.

Until now, we have assumed that any exchange between the Pacific, Atlantic, and Indian oceans occurs via the Southern Ocean. With the rigid lid approximation, this implies that there is negligible mass flux across any latitude for each basin, which completes the determination of our velocity field. The flux of salt given by (14) still implies a net flux of water in reality, but under the rigid lid approximation, the associated divergence in the depth-integrated flow is assumed negligible. That is, the salt flux given by (14) represents the flux divergence associated with the neglected depth-integrated flow; the compensating salt divergence which maintains steady state is achieved through diffusion and the correlation between the salinity variations and the

north-south velocity associated with the overturning circulation. In the previous sections, we have used the latter to infer what the barotropic flow, and hence the water flux, must be. In this section we will generalize the model to explicitly include a barotropic flow.

The modification to the model requires the specification of $w = E - P$ at the surface, plus the addition of the barotropic flow (v and w) to the baroclinic flow used previously. Since the flux divergences associated with the barotropic flow are explicitly represented, the virtual salt flux across the surface is set to zero. Note that since the vertical structure of the velocity field is determined by the thermal wind relation plus the Ekman transport, any depth-integrated flow must be added as a depth-independent component. It should, however, be emphasized that this does not imply that the changes in the flow are depth independent, since the barotropic flow may modify the density field, and hence the vertical structure of the current.

To obtain an appropriate estimate of $E - P$, (14) is used to determine the virtual salt flux, and then this value is divided by the salinity; conversions were done based on both the local surface salinity and a constant value of 35, but the differences were small. When the water flux determined by this method is integrated over the entire ocean surface, the net flux is not guaranteed to vanish. This reflects the fact that for a given surface salinity, there is a unique steady state solution with a given total salt content in the ocean. In our earlier formulation, adjustments to the total salt content were automatically made through the virtual salt flux determined from (14). Since we now specify the water flux across the surface (and hence set the virtual salt flux to zero), there is no mechanism for the total salt content of the ocean to adjust to be consistent with the specified surface conditions. To allow this adjustment, the following modification is made. First, the net salt flux out of the ocean implied by an integration of the virtual salt flux over the entire ocean surface is determined. During the next time step, salt is removed at this rate from the surface layer of the ocean through a spatially uniform change in the surface salinity. This gradually adjusts the total salt content of the ocean to be consistent with the specified surface salinity. As the system approaches a steady state, the global integral of the salt flux tends to zero, and hence the above adjustment vanishes. At every time step the global integral of $E - P$ is adjusted to zero through a spatially uniform change, but due to the relation between $E - P$ and the virtual salt flux, this adjustment also tends to zero as a steady state is approached.

The net volume fluxes through Bering Strait and the Indonesian Passages are specified. Once these fluxes are known, the integrated flux across any other latitude is determined to be consistent with the integral of $E - P$ over the intervening latitudes. Once the barotropic north-south velocity is determined, the associated vertical velocity at interior points is obtained from the continuity equation. This procedure can be applied even if an east-west sill is included in the model, as must be done at both passages.

The above discussion assumes that the model approaches a steady state. In fact, intermittent convection events continue to occur throughout the model runs, so that strictly speaking, only a statistical equilibrium is achieved. These events occur at relatively high frequencies (less than annual time scales) and do not result in significant variations in oceanic conditions. However, if $E - P$ is fixed (e.g., using mixed boundary conditions or coupling to an atmospheric model with a specified hydrological cycle), the small deviations from steady state can lead to dramatic changes, as discussed by *Bryan* [1986] and *Stocker et al.* [1992]. Since we restrict our attention to the relaxation boundary conditions (13) and (14), these interesting effects do not occur in the present study.

To complete the modifications, we include a sill at 50-m depth at the northern end of the Pacific Ocean (Bering Strait). Neglecting storage in the Arctic Ocean, the fluxes of heat and salt through the Bering Strait pass through to the northernmost surface cell of the Atlantic Ocean unaltered. This remains true even if a net flux of water is added to the Arctic, but in this case, an appropriate southward contribution must be added to the velocities in the Atlantic. Similarly, barotropic flow must be explicitly included to allow for the net evaporation in the Mediterranean and Red seas. Exchange between the Pacific and Indian oceans is taken to occur between the equatorial cells via a barotropic flow in the upper 500 m.

A test run, with the exchanges through the Arctic and the Indonesian passages set to zero, so that the barotropic flow was determined entirely by $E - P$, showed negligible changes in either the water mass properties or the thermohaline circulation compared to the same model run based on the earlier formulation.

When a flux of 0.8 Sv through the Bering Strait was included with no addition of water in the Arctic, and no flow through the Indonesian passages, the changes in water mass properties and the baroclinic circulation were small. The broken curves with the second longest dashes in Figure 14 illustrate the effect on the meridional fluxes of heat and salt. The most significant changes are uniform increases in the northward (southward) water flux in the Pacific (Atlantic) basins. The net input of fresh water into the North Atlantic due to the relative freshness of the North Pacific is compensated by a small change in the surface water flux in the northernmost cell of the North Atlantic. Thus, our model results are not sensitive to the exchange through the Bering Strait. This is not surprising, since the exchanges occur in the surface layer, and hence the effects may be compensated effectively by changes in the surface fluxes.

Similarly, we note that by relaxing to observed surface salinities, any freshwater flux that is in reality added to the Arctic, but is neglected from the model, will be mimicked by precipitation in the model North Atlantic. This effect is clearly seen in the plot of meridional water flux for the Atlantic basin shown in Figure 14. The line composed of the longest dashes includes an explicit addition of fresh water to the Arctic at a rate of 0.1 Sv, while the neighboring line of shorter dashes does not. The additional horizontal freshwater flux into the northernmost cell of the North Atlantic simply results in decreased precipitation in this cell in order to maintain the same surface salinity. It should be emphasized that while this has little effect on the oceanic conditions under the relaxation boundary conditions used here, the difference in the hydrological cycle could be important in transient experiments with the surface freshwater flux specified instead of the surface salinity [e.g., *Weaver et al.*, 1991].

Several runs with the Indonesian throughflow varied between 10 and 20 Sv showed that the dominant influence on

the *T-S* properties occurs in the temperature fields of the Pacific and Indian oceans; isotherms are pushed up in the Pacific and pulled down in the Indian Ocean, the largest effect being seen near the equator. The salinity field is affected much less. The associated density changes alter the vertical structure of the current such that the changes in the stream function occur predominantly in the upper 1000 and 500 m of the Pacific and Indian Oceans, respectively. The modifications in the baroclinic flow field have significant effects on the heat and water fluxes, as discussed below.

The final set of results illustrated in Figure 14 (the longest dashes) includes the influence of a 20-Sv volume flux through the Indonesian passages with temperature and salinity taken to be 4°C warmer and 0.5 fresher than the average values for the Pacific equatorial cell. The choices for the temperature and salinity differences are guided by Figure 2 of *Hughes et al.* [1992]. Both the exchange rate and the water mass properties have been deliberately chosen to maximize the influence of the Indonesian throughflow while remaining consistent with the observations. Additional results (not shown) demonstrate that the influence on surface fluxes is further increased if the specified throughflow is more surface intensified.

The influence of the Indonesian throughflow on the surface heat fluxes is relatively small, but the increased southward heat flux in the South Pacific is noteworthy. To explain this rather counterintuitive result, we note that the heat flux estimates shown in Figure 14 were determined by setting the heat flux to zero at the northern extremity of each basin and integrating the surface heat flux to estimate the flux across all other latitudes. This approach is appropriate here, as it corresponds to the method used to obtain the observational heat flux estimates shown in Figures 5, 12, and 14 with which we make comparisons. The northward advection of relatively cold water in the South Pacific actually implies an additional northward heat flux, but the tendency to cool the surface waters must be offset by a net input of heat from the atmosphere. Thus, with the above determination of the heat flux, there is an increased (apparent) southward heat flux in this region and hence improved agreement with the corresponding observational estimates.

As expected, the exchange between the Pacific and Indian oceans influences the estimates of $E - P$ over these basins, again resulting in somewhat better agreement with the observational estimates. However, the large northward water flux estimated for the South Pacific remains in marked contrast with the observational estimates. While this difference could be partly due to errors in the observational estimates of $E - P$, it is likely that the dominant cause is errors associated with zonal variations within each basin, which are not represented by our model.

The above results suggest that the simplification of neglecting interbasin exchanges used in some previous studies is a reasonable first approximation if one is interested in global-scale fluxes of heat and water. We caution, however, that this result is based on a zonally averaged formulation which does not resolve such major features as the Aghulas retroflection and the East Australia Current. Further, all results presented here are based on relaxation boundary conditions, and larger changes might develop under mixed boundary conditions.

A final point of interest is illustrated in Figure 15. In this figure, we have plotted the horizontal heat flux in the Pacific and Indian oceans corresponding to the final plot in Figure 14 (including wind stress, marginal seas, and interbasin exchanges) calculated two different ways. The solid curves are identical to the curves in Figure 14 (determined by setting the heat flux to zero at the northern extremity of each basin and integrating the surface heat flux to estimate the flux across all other latitudes). The dotted curves were determined from the expression

$$\text{heat flux} = \int_{-H}^{0} \rho c_p v' T' a \cos(\phi) \Delta\Lambda dz$$

where a prime indicates a deviation from the depth-averaged value. This estimate ignores the flux associated with net transport through a section, and hence it may be misleading where such transport is significant. It is interesting that previous direct oceanographic calculations of the heat flux in the South Pacific [*Bennett*, 1978; *Georgi and Toole*, 1982; *Wunsch et al.*, 1983] all assume negligible net mass transport and all indicate a very small (possibly positive) meridional heat flux in this region, whereas the bulk formula method indicates a fairly strong southward flux. Figure 15 indicates that the different methods of calculating the heat flux could contribute to this difference.

Hsiung's [1985] results are of interest here, since she obtains much smaller heat flux estimates for the South Pacific using the bulk-formula approach simply by using different surface heat flux estimates. Also of interest is the fact that whereas her heat flux estimates for the South Pacific are low compared to either *Hastenrath*'s [1982] or *Talley*'s [1984] estimates, her estimates for the Indian Ocean are relatively large. Figure 15 indicates that turning the Indonesian throughflow on and off on a time scale too short for baroclinic adjustment to occur might result in heat flux changes with this character (the dotted curve is the heat flux that would result if the throughflow were suddenly terminated). Perhaps, as Hsiung suggests, temporal variations are exceptionally strong in this area. The relation between the Pacific and Indian Ocean flux estimates indicates the possibility that such time dependence could be associated with variations in the flow through the Indonesian Passages.

7. Discussion and Conclusions

There are some weaknesses in the use of zonally averaged equations to represent individual ocean basins. The most obvious is the need to parameterize the east-west density difference in terms of known model quantities: in our case, the north-south density gradient. Further study of results from general circulation models could be undertaken to clarify the intrinsic limitations of this parameterization and to improve on it. In particular, it would be worthwhile to consider how ε changes when the polar halocline catastrophe [*Bryan*, 1986] has resulted in a very weak overturning circulation, and it would be of interest to examine the dependence of ε on other model parameters, particularly K_V and τ^S. It is likely that such studies will show that ε does depend quantitatively on these effects. In this regard, the sensitivity results shown here for ε are particularly encouraging: a factor of 10 change in ε changes the heat and water fluxes in individual basins by less than a factor of 3, and qualitative results are not affected (see Figures 9 and 10).

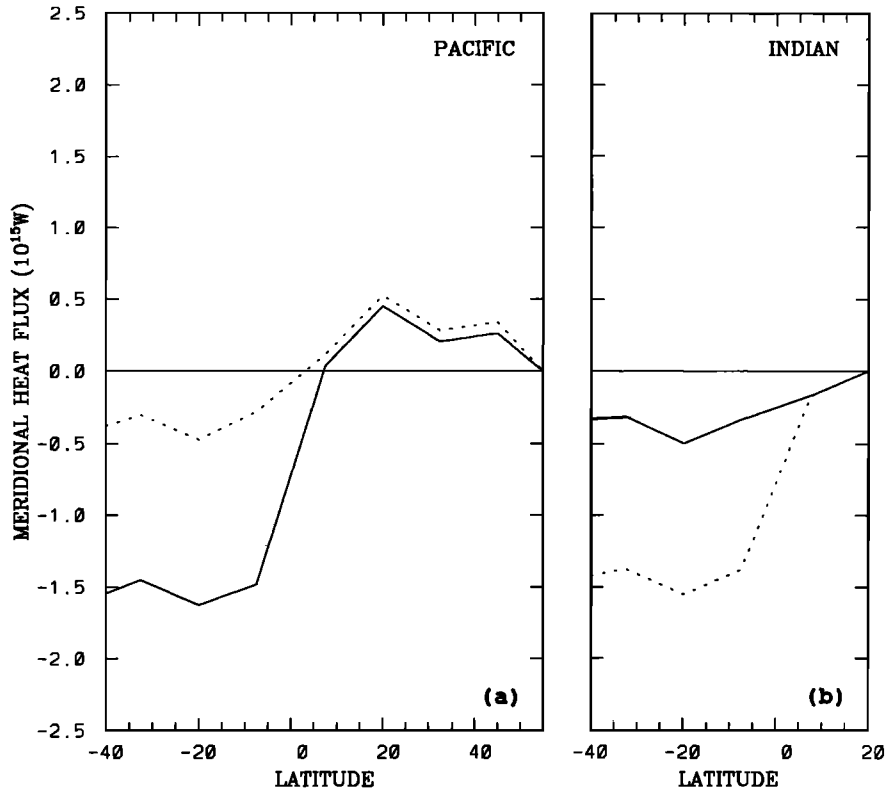

Fig. 15. Heat fluxes based on the model including wind stress, Mediterranean and Red Sea influences, and interbasin exchanges. The solid curves correspond to estimates based on the integrated surface heat flux, and the dotted curves correspond to the depth integral of $v'T'$, where the prime indicates deviation from the depth average.

Nevertheless, this point emphasizes the need to carefully interpret model results.

At least as important as the parameterization of east-west density differences is the neglect of horizontal eddy fluxes of heat and salt, including both the fluxes associated with mesoscale eddies and those associated with the large-scale wind-driven gyres. To some extent, these effects can be represented by eddy diffusion, but this approach is clearly limited, particularly for the large-scale gyre effects. The model is also limited by the lack of resolution of strong boundary currents which can carry water masses over global spatial scales on decadal or shorter time scales. The poor representation of strong advective effects will increase the time scales involved in model simulations of decadal variations. On the other hand, variations in surface water mass properties due to annual and interannual variations in surface fluxes, and the influence of these effects on convective mixing and deep water mass formations, may still be usefully (but cautiously) studied. Further, *Mysak et al.* [1992] have shown that century time scale variability associated with salinity advection may be modeled consistent with OGCM results.

A third weakness of the present model is the treatment of high-latitude processes. In particular, we have made no attempt to include explicit representations of the Arctic Ocean or the Weddell and Ross seas. The omission of the Arctic Ocean does not appear to cause serious problems because the cold temperatures responsible for production of the deep-water masses in the Norwegian and Greenland seas are reflected in the specified annually averaged surface temperatures. However, the high salinities associated with the production of Antarctic Bottom Water are not present in the annually averaged surface salinities, and there is thus no way to produce this water mass without further modifications of the model. We have found that it is possible to create a water mass similar to Antarctic Bottom Water by simply increasing the surface salinity of the most southerly cell in the model, but this approach is clearly ad hoc. Further work on the representation of high latitudes is needed and is a topic of current research (T. F. Stocker et al., The influence of high-latitude forcing on the global thermohaline circulation, submitted to *Paleoceanography*, 1992).

The most obvious conclusion to be drawn from the results presented here is that the present model, based on zonally averaged equations of motion, yields reasonable estimates of the ocean circulation and water mass properties. Probably the greatest uncertainty about the model's ability to represent present-day conditions arises in the determination of the surface fluxes of heat and water, rather than in the determination of the oceanic conditions. This is aggravated here by uncertainty in the data, particularly in the water fluxes. Since global fluxes are probably better determined than individual basin fluxes (both by the model and by the data), and since the net fluxes are of particular interest for climate modeling, it is worthwhile to compare the model and observational estimates of these quantities. Figure 16 shows the comparison for the model estimates corresponding to Figure 11. Evidently, the comparisons for both heat and water fluxes are reasonable. Including explicit representation of the Mediterranean and Red seas and interbasin exchanges improves our model estimates of these quantities rather little. The largest changes associated with these effects are due to the

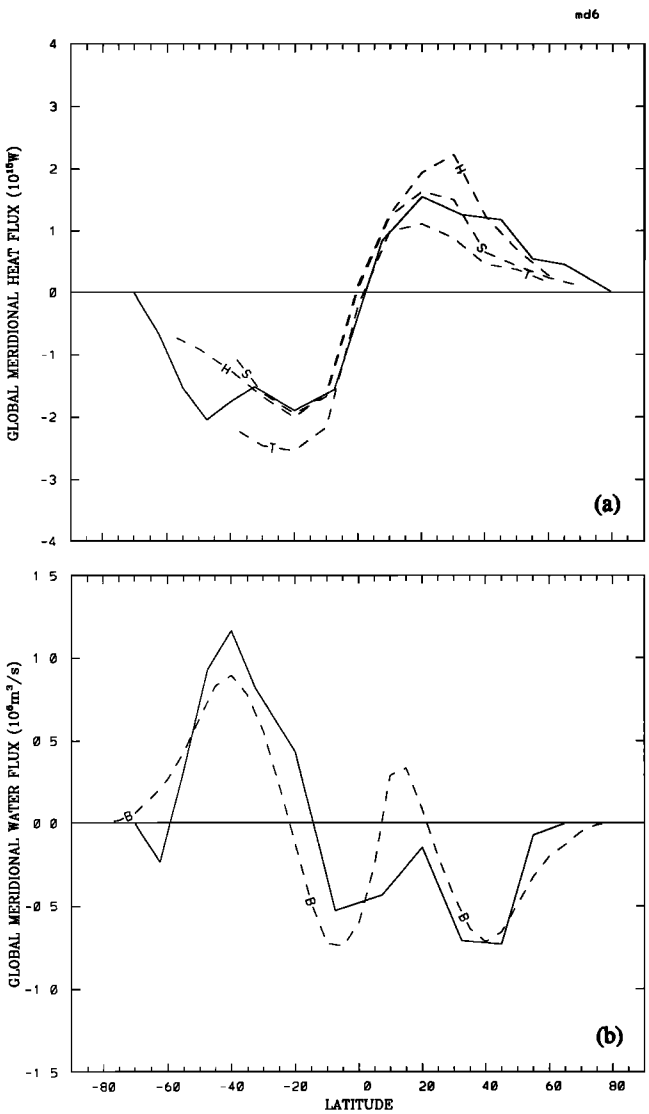

Fig. 16. (*a*) Model estimate of the total heat transport carried by all three ocean basins (solid curve) compared with the observational estimates of *Hastenrath* [1982] (H), *Talley* [1984] (T), and *Hsiung* [1985] (S). (*b*) Model estimate of the total water flux carried by all three ocean basins compared with the water flux estimate of *Baumgartner and Reichel* [1975] (B).

Indonesian throughflow which improves agreement for both quantities, but even here the changes are small.

In addition to reproducing present-day conditions, the model shows sensitivity to parameter variations that are consistent with results from OGCMs. Results are very sensitive to changes in K_V that are within the range of uncertainty in this parameter, and the dependence is similar to that demonstrated for an OGCM by *Bryan* [1986]. Combined with previous studies (WS91, SW91*a*, SW91*b*) which demonstrate that the model reacts to changes in surface fluxes similarly to OGCMs, it appears that the present model is well suited for use in studies of long-term climate changes.

Wind stress significantly improves the agreement with observational estimates of the heat and water fluxes. Larger K_V could improve these flux estimates without including wind stress, but this would degrade the representation of the temperature and salinity fields. In this regard, it is interesting that realistic overturning rates can be achieved for smaller K_V by increasing ε. It seems likely that decreasing horizontal eddy viscosity, A_H, would play an analogous role in OGCMs. Unfortunately, A_H is constrained to take relatively large values in coarse resolution OGCMs by the presence of computational modes. We have not encountered any computational instabilities in our zonally averaged model, provided our time step is sufficiently small. In practice, we take our time step to be about one-fifth of the maximum allowable by the Courant condition in order to remove sensitivity to the time step associated with convective mixing.

K_H has little influence on the model heat and water fluxes, provided it is of the order of 10^3 m^2 s^{-1} or smaller. However, there are some effects of varying K_H within this range that should be mentioned: quantitative changes are small, but since they occur in regions of relatively weak gradients, they are easily observed. These effects are well illustrated by considering the results when Figure 13 is reproduced with K_H reduced to 10^2 m^2 s^{-1}. The first effect is that the deep-water temperatures adjacent to Antarctica are reduced by as much as 1°C as a direct consequence of weaker exchange between this region and the warmer water to the north. Consistent with this change, the low-salinity deep water produced in the cell adjacent to Antarctica has less effect on the deep waters to the north, and the deep salinities are thus increased by order 0.1 in the Pacific and Indian oceans. Finally, with the smaller diffusion coefficient, the salinity signature of the Antarctic Intermediate Water intrusions into the Pacific and Indian oceans is more realistically represented. This latter point may seem surprising, as one might expect horizontal diffusion to aid the spread of Antarctic Intermediate Water into the basins. However, the upwelling in the equatorial regions of both the Pacific and the Indian oceans supplies relatively saline deep water which can mix with the fresher intruding Antarctic Intermediate Water to destroy its signature in the salinity field. By reducing K_H, the signature of this water mass is preserved with very minimal changes in other model results.

Explicit representation of the vertical exchange associated with the Mediterranean and Red seas significantly improves estimates of the *T-S* properties in both the Atlantic and Indian oceans, but has little influence on the estimates of the meridional heat and water fluxes.

Exchange through the Bering Strait has little effect on the model estimates of the ocean circulation, water mass properties, or air-sea exchanges of heat and water. On the other hand, a 20-Sv flow through the Indonesian passages does influence the model estimates of the individual heat and water fluxes carried by the Pacific and Indian oceans, and results in somewhat better agreement with observational estimates. Further, it has been demonstrated that simply neglecting the heat flux associated with the net northward transport in the South Pacific results in much lower heat flux estimates than those estimated by the bulk formula method, similar to results obtained by direct methods. Both of these results support the contention that there is a large flux through these passages. While these results suggest that the Indonesian throughflow has important effects in the Pacific and Indian oceans, the net effect on the global meridional heat and water fluxes carried by all three basins is small.

Appendix A: Convective Overturning Scheme

When unstable stratification develops, it must be removed by some mixing scheme which parameterizes the influence

of small-scale motions not resolved by the model. When pressure dependence of the equation of state is neglected, an efficient mixing scheme is achieved by simply determining the top and bottom cells in unstable parts of the water column and setting the temperature and salinity to the volume-weighted mean over this region. This procedure is repeated until no unstable regions remain. (Note that the repetition is required due to possible cabbeling associated with the nonlinear dependence of density on T and S).

When pressure dependence is included in the equation of state, stability must be determined with respect to the in situ density, and the simple approach described above is inappropriate. In this case, we have used the following scheme, which includes all nonlinear effects, is computationally efficient, and results in a stable water column at the end of each time step.

Let k represent the vertical index of a grid cell in the model with $k = 1$ at the bottom and $k = N$ at the top. Starting at $k = N$, determine the in situ density of cells k and $k - 1$ at the pressure level separating the two cells. If the stratification is stable, reduce k by 1 and repeat the procedure on the next pair of cells. If for some k the stratification is neutrally stable or unstable, assign the mass-weighted mean salinity and potential temperature (referenced to the surface) to each of the two cells, and store the index of the upper cell and the total thickness of the mixed region in k_0 and h_0, respectively. Again, reduce k by 1 and check the vertical stability of the next two cells using the new potential temperature and salinity values for the upper cell. If these cells are unstable, then mix the lower cell with the upper region of thickness h_0. Reset the salinity and potential temperature of all cells between k_0 and $k - 1$ to the appropriate mean value, and reset h_0 to the new thickness of the mixed region. Do not modify the value of k_0. In this way, the lower cell is effectively mixed into the preexisting well-mixed region and the parameters of the mixed region are updated with minimal computation. Continue checking the stability of subsequent cells and mixing the whole unstable range of cells until a level is reached where the initial stratification is stable between levels k and $k - 1$. If such a stable region is found, reset k_0 to $k - 1$ and h_0 to the thickness of this single cell and continue the process until the bottom is reached. If necessary, sweep through the column several times until it is found that no regions of unstable stratification occur. In practice, we allowed a maximum of four sweeps in our program, but test cases suggest that the water column is generally stable after the second sweep.

Appendix B: The Southern Ocean Ridge

In the main body of the text we have simply used a small value of ε (=0.0001) at the southern cell boundary, where there are no meridional barriers to obstruct zonal flow. This choice reflects the fact that in the absence of such barriers, the average north-south geostrophic flow around a latitude belt must vanish. The very small value of ε was included for computational convenience, and the meridional exchange is determined primarily by horizontal diffusion. In reality, at this latitude band there are several subsurface meridional ridges which can support east-west pressure differences and consequently a geostrophically balanced overturning circulation. This geostrophic flow is believed to be important in the northward transport of Antarctic Bottom Water. We now show how to include this component of the overturning circulation in our model.

We begin by allowing nonzero Δp at levels below the crest of the ridge, but insist that $\Delta p \equiv 0$ for all points above the crest. Below the crest, (10) holds. Using the hydrostatic equation and generalizing to allow ε to be an arbitrary function of depth, this gives

$$\left(\frac{\Delta p}{\Delta \Lambda}\right)_z = -2\varepsilon(z)sc\,\frac{\partial \rho}{\partial \phi} \tag{B1}$$

Integrating (B1) from the bottom to an arbitrary level z, we obtain the relation

$$\frac{\Delta p}{\Delta \Lambda} = \left.\frac{\Delta p}{\Delta \Lambda}\right|_{-H} + 2scg\int_{-H}^{z} \varepsilon(\xi)\rho_\phi\, d\xi \qquad -H \le z \le -H + H_R \tag{B2}$$

$$\frac{\Delta p}{\Delta \Lambda} = 0 \qquad z > -H + H_R$$

where H_R is the height of the ridge above the bottom. If we now substitute (B2) into (1) and integrate over the water column, we obtain an expression for $\Delta p/\Delta\Lambda$ at $z = -H$:

$$\left.\frac{\Delta p}{\Delta \Lambda}\right|_{-H} = \frac{1}{H_R}\left\{2scg\int_{-H}^{-H+H_R} \varepsilon(\xi)(\xi + H - H_R)\rho_\phi\, d\xi + ac\tau^s + 2\rho_* asc\Omega V\right\} \tag{B3}$$

where V represents the depth integral of the zonally averaged north-south velocity component through the section. If the rigid lid approximation is made, V is set to zero, and flux divergences associated with the barotropic flow are represented by the surface boundary conditions. Substituting (B3) into (B2) and using the resulting equation in (1), we obtain

$$v = \frac{g}{\Omega a H_R}\left\{\int_{-H}^{-H+H_R} \varepsilon(\xi)(\xi + H)\frac{\rho_\phi}{\rho_*}\, d\xi - \int_{z}^{-H+H_R} \varepsilon(\xi) H_R \frac{\rho_\phi}{\rho_*}\, d\xi\right\} + \frac{V}{H_R} - \frac{\tau^s}{2\Omega\rho_* s}\cdot\left(\frac{\mathcal{H}(z + H_M)}{H_M} - \frac{1}{H_R}\right) \qquad -H \le z \le -H + H_R \tag{B4}$$

$$v = -\frac{\tau^s}{2\Omega\rho_* s H_M}\,\mathcal{H}(z + H_M) \qquad z > -H + H_R$$

The stream function may now be determined by integrating (17a), and w can be determined using (17b).

The formulation for a deep meridional ridge was used only for the runs discussed in section 6. We chose a constant value of $\varepsilon = 0.15$ beneath a ridge crest at 2500-m depth at the latitude band separating cells 1 and 2 in Figure 1. The choice of ε corresponds to a zonal separation of 120° between ridges, a crude but not unreasonable representation of reality. The resulting zonally integrated overturning circulation corresponding to Figure 13, for latitudes south of 40°S, is

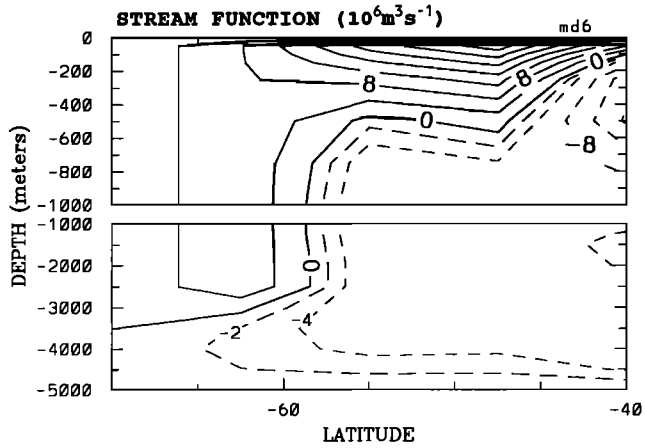

Fig. 17. The zonally averaged meridional circulation south of 40°S corresponding to Figure 13. This run includes a meridional ridge below 2500 m for latitudes south of 55°S. When a ridge is not included, the meridional circulation across the cell boundary at 65°S consists of the surface Ekman flux and a nearly depth-independent return flow. The reversed circulation near the bottom is totally absent.

shown in Figure 17. As expected, there is a northward bottom flow which helps transport Antarctic Bottom Water away from the continent.

Finally, we note that if $H_R = H$, then (B4) reduces to (16). The generalization to a depth dependent ε has been included for generality, but it has not been used in any of our model runs.

Acknowledgments. We are grateful to Allyn Clarke for several useful discussions regarding global ocean circulation and watermass properties. Comments by John Lazier, Allyn Clarke, and two JGR reviewers helped improve the presentation. This study was partially funded by the Natural Sciences and Energy Research Council of Canada and the Swiss National Science Foundation.

REFERENCES

Aagaard, K., and E. C. Carmack, The role of sea ice and other fresh water in the Arctic circulation, *J. Geophys. Res.*, *94*, 14,485–14,498, 1989.

Baumgartner, A., and E. Reichel, *The World Water Balance*, 179 pp., Elsevier, New York, 1975.

Bennett, A. F., Poleward heat fluxes in southern hemisphere oceans, *J. Phys. Oceanogr.*, *8*, 785–798, 1978.

Boyle, E. A., and L. D. Keigwin, Deep circulation of the North Atlantic over the last 200,000 years: Geochemical evidence, *Science*, *218*, 784–787, 1982.

Boyle, E. A., and L. D. Keigwin, North Atlantic thermohaline circulation during the past 20,000 years linked to high-latitude surface temperature, *Nature*, *330*, 35–40, 1987.

Broecker, W. S., and G. H. Denton, The role of ocean-atmosphere reorganizations in glacial cycles, *Geochim. Cosmochim. Acta*, *53*, 2465–2501, 1989.

Bryan, F., High-latitude salinity effects and interhemispheric thermohaline circulations, *Nature*, *323*, 301–304, 1986.

Bryan, F., Parameter sensitivity of primitive equation ocean general circulation models, *J. Phys. Oceanogr.*, *17*, 970–985, 1987.

Bryan, K., and L. J. Lewis, A water mass model of the world ocean, *J. Geophys. Res.*, *84*, 2503–2517, 1979.

Bryden, H. L., and H. M. Stommel, Limiting processes that determine basic features of the circulation in the Mediterranean Sea, *Oceanol. Acta*, *7*, 289–296, 1984.

Bryden, H. L., D. H. Roemmich, and J. A. Church, Ocean heat transport across 24°N in the Pacific, *Deep Sea Res.*, *38*, 297–324, 1991.

Coachman, L. K., and K. Aagaard, Transports through Bering Strait: Annual and interannual variability, *J. Geophys. Res.*, *93*, 15,535–15,539, 1988.

Cox, M. D., An idealized model of the world ocean, Part I, The global-scale water masses, *J. Phys. Oceanogr.*, *19*, 1730–1752, 1989.

Cummins, P. F., G. Holloway, and A. E. Gargett, Sensitivity of the GFDL Ocean General Circulation Model to a parameterization of vertical diffusion, *J. Phys. Oceanogr.*, *20*, 817–830, 1990.

Duplessy, J. C., N. J. Shackleton, R. G. Fairbanks, L. Labayrie, D. Oppo, and N. Kallel, Deepwater source variations during the last climatic cycle and their impact on the global deepwater circulation, *Paleoceanography*, *3*, 343–360, 1988.

Fieux, M., C. Andrié, A. Kartavtseff, P. Delecluse, and R. Molcard, Measurements within the Pacific–Indian Ocean throughflow region: Preliminary results of the Jade cruise, paper presented at the 20th General Assembly, Int. Union Geod. and Geophys., Vienna, 1991.

Gargett, A. E., Vertical eddy diffusivity in the ocean interior, *J. Mar. Res.*, *42*, 359–393, 1984.

Georgi, D., and J. Toole, The Antarctic Circumpolar Current and the oceanic heat and freshwater budgets, *J. Mar. Res.*, *40*, Suppl., 183–197, 1982.

Gill, A. E., *Atmosphere-Ocean Dynamics*, 662 pp., Academic, San Diego, Calif., 1982.

Godfrey, S., and T. J. Golding, The Sverdrup relation in the Indian Ocean, and the effect of Pacific–Indian Ocean throughflow on Indian Ocean circulation and on the East Australian Current, *J. Phys. Oceanogr.*, *11*, 771–779, 1981.

Gordon, A. L., Interocean exchange of thermocline water, *J. Geophys. Res.*, *91*, 5037–5046, 1986.

Gregg, M. C., Diapycnal mixing in the thermocline: A review, *J. Geophys. Res.*, *92*, 5249–5286, 1987.

Hall, M. M., and H. L. Bryden, Direct estimates and mechanisms of ocean heat transport, *Deep Sea Res.*, *29*, 339–359, 1982.

Han, Y. J., and S. W. Lee, An analysis of monthly mean wind stress over the global ocean, *Mon. Weather Rev.*, *111*, 1554–1566, 1983.

Hastenrath, S., On the meridional heat transport in the world ocean, *J. Phys. Oceanogr.*, *12*, 922–927, 1982.

Hsiung, J., Estimates of global oceanic meridional heat transport, *J. Phys. Oceanogr.*, *15*, 1405–1413, 1985.

Hughes, T., A. J. Weaver, and J. S. Godfrey, Thermohaline forcing of the Indian Ocean by the Pacific Ocean, *Deep Sea Res.*, in press, 1992.

Ikeda, M., Wind effects on the buoyancy-driven general circulation in a closed basin using a two-level model, *J. Phys. Oceanogr.*, *17*, 1707–1723, 1987.

Lacombe, H., and C. Richez, The regime of the Strait of Gibraltar, in *Hydrodynamics of Semi-Enclosed Seas*, edited by J. C. J. Nihoul, pp. 13–74, Elsevier, New York, 1982.

Levitus, S., Climatological atlas of the world ocean, *NOAA Prof. Pap.*, *13*, 173 pp., 1982.

Maier-Reimer, E., and U. Mikolajewicz, Experiments with an OGCM on the cause of the Younger Dryas, *Rep. 39*, 13 pp., Max-Planck-Inst. für Meteorol., Hamburg, Germany, 1989.

Manabe, S., and R. J. Stouffer, Two stable equilibria of a coupled ocean-atmosphere model, *J. Clim.*, *1*, 841–866, 1988.

Marotzke, J., Instabilities and steady states of the thermohaline circulation, in *Ocean Circulation Models: Combining Data and Dynamics*, edited by D. L. T. Anderson and J. Willebrand, pp. 501–511, Kluwer, The Hague, Netherlands, 1989.

Marotzke, J., and J. Willebrand, Multiple equilibria of the global thermohaline circulation, *J. Phys. Oceanogr.*, *21*, 1372–1385, 1991.

Marotzke, J., P. Welander, and J. Willebrand, Instability and multiple equilibria in a meridional-plane model of the thermohaline circulation, *Tellus*, *40A*, 162–172, 1988.

Munk, W. H., Abyssal recipes, *Deep Sea Res.*, *13*, 707–730, 1966.

Mysak, L. A., T. F. Stocker, and F. Huang, Century scale variability in a randomly forced two dimensional thermohaline ocean circulation model, *Clim. Dyn.*, in press, 1992.

Rooth, C., Hydrology and ocean circulation, *Progr. Oceanogr.*, *11*, 131–149, 1982.

Rooth, C., and H. G. Ostlund, Penetration of tritium into the Atlantic thermocline, *Deep Sea Res.*, *19*, 481–492, 1972.

Siedler, G., Schichtungs- und Bewegungsverhältnisse am Südaus-

gang des Roten Meeres, *Meteor Forschungsergeb. Reihe A*, *4*, 1, 1968.

Siedler, G., General circulation of water masses in the Red Sea, in *Hot Brines and Recent Heavy Metal Deposits in the Red Sea*, edited by E. T. Degens and D. A. Ross, Springer-Verlag, New York, 1969.

Smolarkiewicz, P. K., A simple positive definite advection scheme with small implicit diffusion, *Mon. Weather Rev.*, *111*, 479–486, 1983.

Stocker, T. F., and D. G. Wright, A zonally averaged ocean model for the thermohaline circulation, II, Interocean circulation in the Pacific-Atlantic basin system, *J. Phys. Oceanogr.*, *21*, 1725–1739, 1991*a*.

Stocker, T. F., and D. G. Wright, Rapid transitions of the ocean's deep circulation induced by changes in surface water fluxes, *Nature*, *351*, 729–732, 1991*b*.

Stocker, T. F., D. G. Wright, and L. A. Mysak, A zonally averaged, coupled ocean-atmosphere model for paleoclimate studies, *J. Clim.*, in press, 1992.

Stommel, H., Thermohaline convection with two stable regimes of flow, *Tellus*, *13*, 224–230, 1961.

Talley, L. D., Meridional heat transport in the Pacific Ocean, *J. Phys. Oceanogr.*, *14*, 231–241, 1984.

Weaver, A. J., and E. S. Sarachik, Evidence of decadal variability in an ocean general circulation model: An advective mechanism, *Atmos. Ocean*, *29*, 197–231, 1991*a*.

Weaver, A. J., and E. S. Sarachik, The role of mixed boundary conditions in numerical models of the ocean's climate, *J. Phys. Oceanogr.*, *21*, 1470–1493, 1991*b*.

Weaver, A. J., E. S. Sarachik, and J. Marotzke, Freshwater flux forcing of decadal/interdecadal oceanic variability, *Nature*, *353*, 836–838, 1991.

Welander, P., Thermohaline effects in the ocean circulation and related simple models, in *Large-Scale Transport Processes in Oceans and Atmosphere*, edited by J. Willebrand and D. L. T. Anderson, pp. 163–200, D. Reidel, Hingham, Mass., 1986.

Wijffels, S. E., R. W. Schmitt, H. L. Bryden, and H. Stigebrandt, Transport of freshwater by the oceans, *J. Phys. Oceanogr.*, *22*, 155–162, 1992.

Wright, D. G., and T. F. Stocker, A zonally averaged ocean model for the thermohaline circulation, I, Model development and flow dynamics, *J. Phys. Oceanogr.*, *21*, 1713–1724, 1991.

Wunsch, C., An eclectic Atlantic Ocean circulation model, I, The meridional flux of heat, *J. Phys. Oceanogr.*, *14*, 1712–1733, 1984.

Wunsch, C., D. Hu, and B. Grant, Mass, heat, salt, and nutrient fluxes in the South Pacific Ocean, *J. Phys. Oceanogr.*, *13*, 725–753, 1983.

T. F. Stocker, Lamont-Doherty Geological Observatory, Columbia University, Palisades, NY 10964.

D. G. Wright, Department of Fisheries and Oceans, Physical and Chemical Sciences, Bedford Institute of Oceanography, Dartmouth, Nova Scotia, Canada B2Y 4A2.

(Received October 18, 1991;
revised March 17, 1992;
accepted May 8, 1992.)